ISSN 1075-7015, Geology of Ore Deposits, 2019, Vol. 61, No. 1, pp. 50–73. © Pleiades Publishing, Ltd., 2019.
Russian Text © N.E. Savva, A.V. Volkov, A.A. Sidorov, E.E. Kolova, K.Yu. Murashov, 2019, published in Geologiya Rudnykh Mestorozhdenii, 2019, Vol. 61, No. 1.

Primorskoe Epithermal Ag–Au Deposit (Northeastern Russia): Geological Setting, Mineralogy, Geochemistry, and Ore Formation Conditions

N. E. Savva[a], A. V. Volkov[b], *, A. A. Sidorov[b], E. E. Kolova[a], and K. Yu. Murashov[b]

[a] *Northeastern Interdisciplinary Scientific Research Institute, Far East Branch, Russian Academy of Sciences, Magadan, 685000 Russia*

[b] *Institute of Geology of Ore Deposits, Petrography, Mineralogy, and Geochemistry, Russian Academy of Sciences, Moscow, 119017 Russia*

**e-mail: tma2105@mail.ru*

Received September 11, 2017; revised May 29, 2018; accepted June 7, 2018

Abstract—The potentially large Primorskoe epithermal Au–Ag deposit is represented by three areas: the Kholodnyi, Spiridonych, and Teplyi. It is located in the Omsukchan district of Magadan oblast, where mining is carried out at the largely similar Dukat, Lunnoe, Gol'tsovoe, Arylakh, Tidit, Pereval'noe, and other deposits. The deposit under review is located in the Kalalaga volcano-tectonic depression, where ore has been emplaced in a gently dipping sequence of Late Cretaceous ignimbrites and rhyolites more than 700 m in thickness crosscut by numerous intermediate and mafic dykes. According to drilling data, there is a leucocratic granite massif 400–500 m beneath the deposit, which is exposed on the surface in the northeastern part of the ore field. The presence of Bi-bearing galena and matildite, as well as medium- to high-temperature metasomatic facies (epidote and actinolite) and the specific physicochemical conditions of epithermal Ag–Au ore emplacement, attests to the above-intrusion position and the role of granitoids as high-temperature magmatic fluid generators responsible for supplying Bi and heating the host rock. The ore chemistry is quite consistent with its mineral composition. High Mn and Ag; elevated Au; low Cu, Pb, Zn, Sb, As, Bi, and Te; and low total REE concentrations were established, along with negative Eu and positive Ce anomalies. The high Te/Se, Sr/Ba, Y/Ho, and U/Th ratios in the ores are due to their location in the area influenced by the granitoid pluton. The physicochemical parameters of ore emplacement in the Teplyi area are unusual: high temperatures, low salt concentrations, and fluid densities typical of a "dry vapor" environment. The obtained data allow the Primorskoe to be classified as an intermediate sulfidation epithermal deposit. The data discussed below are of practical use for regional metallogenic forecasting, exploration, and economic assessment of epithermal Ag–Au deposits.

Keywords: northeastern Russia, Omsukchan zone, Primorskoe, epithermal, deposit, silver, gold, pyrolusite, structure, ore mineralogy, geochemistry, fluid inclusions, genesis

DOI: 10.1134/S1075701519010069

INTRODUCTION

Epithermal Au–Ag deposits in many cases comprise volcano-plutonic systems of combined preintrusion and postintrusion groups of preporphyry and postporphyry deposits in a series of volcanogenic ore formations (Sidorov et al., 2011). In this respect, the Primorskoe deposit is a specific topic that makes it possible to review problematic genetic issues of epithermal mineralization.

The Primorskoe deposit, as represented by three areas (the Kholodnyi, Spiridonych, and Teplyi), is located in the southern part of the Omsukchan district of Magadan oblast, 22 km from the Sea of Okhotsk and 360 km northeast of Magadan (Fig. 1, inset). The distance from the deposit to the operating ore concentration plant in the village of Omsukchan is 215 km.

The deposit was discovered in 1978 by geologists of the Khasyn geological exploration expedition sent to confirm geochemical anomalies revealed by geochemical surveys of dispersion trains on a scale of 1 : 200000. Exploration operations were carried out by the Dukat geological exploration expedition from 1981 to 1987. Later (2006), exploration and development rights for the deposit were licensed to the federal state unitary enterprise (FGUP) Magadangeologiya, which resumed exploration operations in the rich Teplyi area in 2008–2009. The license was transferred to OJSC Polimetall UK in July 2015. Based on exploration data obtained by this company, the total resources of just two orebodies at the Primorskoe deposit as of 2017

were estimated at about 2 t gold (in ores with an average grade of 4 g/t Au) and 600 t silver (1216 g/t Ag). The total resource potential of all three areas of the deposit, according to Magadangeologiya, is 21 t gold and 5000 t silver.

Since its discovery date, the geological setting and mineral composition of the ores at this deposit have been studied at the Central Geological Research Institute for Nonferrous and Precious Metals (TsNIGRI) (Struzhkov and Konstantinov, 2005) and later at Magadangeologiya. Mineralogical–geochemical and thermobarogeochemical (fluid inclusion) studies of ores from the Teplyi area were carried out in 2014–2016 at the Northeastern Interdisciplinary Scientific Research Institute, Far East Branch, Russian Academy of Sciences (SVKNII FEB RAS) and the Institute of Geology of Ore Deposits, Petrography, Mineralogy, and Geochemistry of the Russian Academy of Sciences (IGEM RAS) under project no. 14–17–00170 of the Russian Science Foundation. This paper summarizes the results of integrated studies of the deposit.

RESEARCH METHODS

The section Geological Setting was prepared at IGEM RAS based on archival and published data integrated with original findings. Wall-rock metasomatites, ore structures, and composition were studied (reflected light microscopy of numerous polished ore specimens under an Axioplan Imaging microscope) and fluid inclusion (FI) microthermometry was carried out at SVKNII FEB RAS. Ore mineral compositions were determined with a Camebax X-ray electron-probe microanalyzer equipped with an Oxford Instruments INCA add-on device (analysts E.M. Goryacheva and T.V. Subbotnikova at SVKNII FEB RAS, Magadan, and I.A. Bryzgalov at Moscow State University).

FI microthermometry was carried out with measurement system consisting of a Linkam THMSG600 heating/freezing microscope stage, a Motic microscope equipped with an Olympus 50X objective lens with a long working length, a Moticam 3 video camera, and a control computer. The salt concentration in FIs was estimated from the ice melting temperature—$Tm_{(ice)}$—using data from (Bodnar and Vityuk, 1994). The salt composition of fluids was estimated from eutectic temperatures (Borisenko, 1977) or by analysis of water extracts (WE) prepared according to (Kryazhev et al., 2006) and analyzed on an Agilent4100 MP atomic emission spectrometer at SVKNII FEB RAS. Inelastic (Raman) scattering spectroscopy was carried out with a LabRAM HR Raman microscope in a wide spectral range of 150–3800 cm^{-1} with the 514 nm excitation line of a He–Ne laser and a spectral slit width of 2 cm^{-1} (analyst E.E. Kolova). Composite contours were decomposed with Origin 7.5 software. Salinity and water vapor pressure were estimated with FLINCOR software (Brown, 1989).

Rock-forming and some foreign element concentrations in ores were determined by X-ray fluorescence analysis at the Analytical Laboratory of IGEM RAS with a PANalytical Axios mAX wavelength-dispersive vacuum spectrometer. The spectrometer was calibrated against industry-specific and national standard samples of the chemical compositions of rocks. Analysis was carried out following the 439-RS NSAM VIMS method, which ensures compliance of the results with the OST RF 41-08-205-04 industrial standard (analyst A.I. Yakushev). Trace element concentrations were measured with an X-Series II ICP-MS mass spectrometer after the sample was ionized with inductively coupled plasma (analyst Ya.V. Bychkova). The detection limits ranged from 0.1 ng/g for heavy and medium-weight elements to 1 ng/g, for light elements. The uncertainty of analysis was 1–3% RPD. Gold grades of samples were determined by atomic absorption spectrometry with electrothermal atomization using a Spectr AA 22OZ spectrometer (analyst V.A. Sychkova). Geochemical indicator values were determined to study the ore formation conditions. The obtained values were tabulated and used to plot the REE and TR distribution curves for the studied ores.

GEOLOGICAL SETTING

The Primorskoe deposit is located in the Omsukchan volcanic trough of the Okhotsk–Chukotka volcanic belt (OCVB) in the zone, where it overlaps the Uda–Murgali island arc (UMIA). These structural zones coinside in strike with two major metallogenic zones, the roughly N–S trending Omsukchan zone characterized by Sn, Ag, Pb, and Zn deposits and the NE–SW trending Uda–Murgali characterized by Cu and Mo deposits. The geological section of the Primorskoe area consists of Jurassic marine clastics, Upper Cretaceous surface volcanic and volcano-sedimentary deposits, and a thin cover of loose Quaternary sediments. The oldest rocks (J) are exposed in the crestal area of the Aliki intrusive dome in the northern part of the area. They consist of a monotonic sequence of fossil-barren dark gray silicified oligomictic and polymictic siltstones warped into small compound folds.

Upper Cretaceous (K_2) volcanic and volcano-sedimentary deposits that rest unconformably on the Jurassic marine deposits are the most widespread stratified deposits in the region. They are related to the OCVB, fill depressions and sinks in volcanic grabens, and comprise eruptive and subvolcanic facies that differ in emplacement conditions and mode of occurrence. Eruptive facies proper include lava and pyroclastic flows (sheets) and synchronous volcano-sedimentary deposits. In terms of composition, the stratified volcanic rocks of the study area are subdi-

vided into four series: basaltic andesite, dacite, andesite, and rhyolite.

Intrusive facies of the Late Cretaceous volcano-plutonic complex vary in composition. They are widespread and occupy about 30% of the area under review. These facies include subvolcanic, plutonic, and dyke complexes intruded in Jurassic and Upper Cretaceous stratified rocks.

Rocks that make up subvolcanic and volcanic neck bodies are considered age equivalents of stratified volcanic rocks of similar composition with gradual transitions to the former. Intrusive rocks are holocrystalline rocks varying from gabbro to granite, which make up the large Aliki, Tik, Kalalaga, and Viliga polygenetic massifs and a series of small stocks that can be interpreted as dome-shaped protrusions or satellites of the large massifs not exposed by erosion. The massifs are multiphase—gabbro–diorite, granodiorite, granite, and basalt phases were recognized. In addition, the intrusive complex comprises dyke suites of various compositions both inside the massifs and in the immediately adjacent aureoles. The dykes are 1–2 to 80–100 m thick and 100–2500 m long.

The Kalalaga volcano-tectonic depression, where the Primorskoe deposit is located, is ovate (17 × 20 km) and surrounded by intrusions. The long axis of the depression is NE trending (20°–30°). The inner structure of the depression is asymmetrical. The Neokolchan–Kalalaga graben divides the depression into three parts. Granites of the Kalalaga massif are exposed in its eastern part as a ring-shaped protrusion, which is NE trending in this part. The contacts of the massif dip at 40°–60° toward the center of the structure.

Located within the graben is the isometric core (inner sink) of the structure, approximately 7 km in diameter. Flat-lying volcanic rocks of the rhyolite series are exposed in the core.

The southern and southwestern surroundings of the central sink display outcrops of subvolcanic polyphyric rhyolite porphyry (nevadite) bodies—the roots of lava sheets of the rhyolite series. In the central part, the Krivoi fault divides the core into two areas, Teplyi and Molot, in which the respective areas of the Primorskoe deposit are located. The Kholodnyi and Spiridonych areas are located in the northern part of the Kalalaga volcano-tectonic structure (Fig. 1).

The northwestward elongation of the ore field reflects the strike of the principal ore-controlling structure—the central branch of the Omsukchan deep-seated fault. The main orebodies are oriented in the same direction (Fig. 1). In general, the orientations of both the ore stockwork and ore-bearing block within the field are controlled by three systems of faults—northwest trending, northeast trending, and E–W trending. Ore-bearing areas that make up a single ore zone are split into blocks by northeast trending faults characterized by dextral strike-slip displacement along them (Fig. 1).

Exploration operations in the *Spiridonych area* led to the recognition of five carbonate–quartz stockwork zones confirmed over a distance of 1–2.5 km with a thickness of 5–7 to 35–40 m. Surface outcrops of these zones are characterized by low grades of valuable components.

The *Kholodnyi area* contains at least two northeast trending, high-dipping orebodies. The orebodies are hosted by silicified ignimbrites and accompany andesite dykes. Based on grab sampling data, ore grades are up to 10.6 g/t gold and 2276.3 g/t silver.

At present, detailed exploration is under way in the *Teplyi area*, which covers 10 km^2 (Fig. 1). The area is underlain by Late Cretaceous stratified volcanic rocks crosscut by intusive bodies of various composition, morphology, and formation conditions. The geological section begins with volcaniclastic series is ubiquitous within the area (Fig. 1); it consists of psammitic and psephitic rhyolitic ignimbrites interbedded with rhyolite tuffs, basalts, trachyandesites, and their tuffs. The sequence is more than 700 m in thickness; the dip of the stratified rocks is gently centriclinal (Fig. 3).

The largest intrusive body in the area is composed of subalkaline leucocratic amphibole–biotite granites of the main phase of the Kalalaga massif, exposed along the northeastern and southwestern boundaries of the area (Fig. 1, Fig. 3). Diorite bodies crosscut all stratified volcanic rocks (Fig. 3); they are metamorphosed at the contact with the granites.

The area is characterized by a high abundance of dykes of various compositions. Subalkaline basalts, less frequently diorites and diorite porphyries, make up the northeast trending (45°–60°) dyke belts. The earliest (preore) ones are subalkaline basalt and basaltic andesite dykes as well as northwest trending early rhyolite and trachyrhyodacite dykes. Post-ore dykes are represented mostly by northeast trending subalkaline basalt and granite porphyry bodies. Significant displacements of orebodies along these dykes were not established except for the northern part of orebody no. 3, which was found to be offset 40–50 m northeastward along a thick linear granite porphyry dyke.

The structure of the area is defined by two mutually perpendicular northeast trending and northwest trending fault systems. The northwest trending faults are regional-scale and extend over distances of 3.0–3.5 km; they lie 500–600 m apart. One of them hosts ore zones 1 and 3; the other, ore zone 16; and the third one, ore zones 5 and 6. The faults dip steeply northeastward. Ore zones are accompanied by silver, lead, zinc, and manganese geochemical anomalies. Rb/Sr age of mineralization is Late Cretaceous (72 ± 6 Ma) (Struzhkov and Konstantinov, 2005).

More than 30 veins and stockworks were recognized in the Teplyi area. Notwithstanding their large number, veins exhibit uniform sets of barren and ore-bearing components and differ only in structure and Au/Ag ratio. The main veins (~1–2 m in thickness)

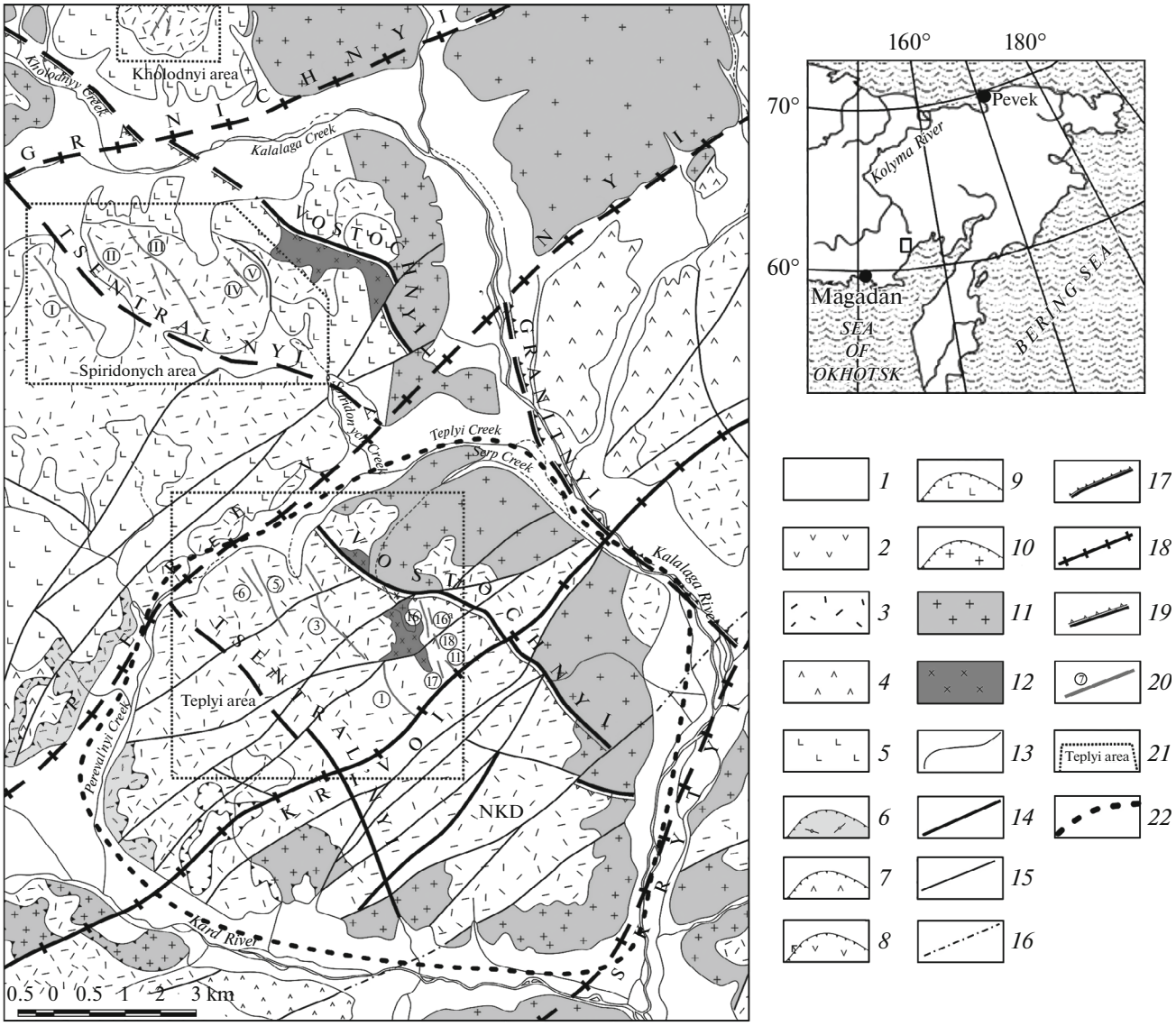

Fig. 1. Schematic geological map of Primorskoe deposit (modified after Magadangeologiya archival data). (*1*) Quaternary sediments; (*2*) andesite series; (*3*) rhyolite series; (*4*) dacite series; (*5*) basaltic andesite series. *Volcanic bodies:* (*6*) rhyolite; (*7*) dacite; (*8*) andesite; (*9*) basalt; (*10*) porphyry granite. *Intrusions:* (*11*) granite; (*12*) diorite; (*13*) geological boundaries. *Faults and fault names:* (*14*) major; (*15*) minor; (*16*) cryptic, hidden under Quaternary sediments; (*17*) peripheral caldera fault; (*18*) radial caldera faults; (*19*) peripheral normal faults of Neokolchan–Kalalaga district (NKD); (*20*) stockworks and veins and their numbers; (*21*) area boundaries and names; (*22*) outline of core of Kalalaga volcanic structure.

are accompanied by argentiferous stockwork zones that considerably thicken the orebodies. Veins are steeply dipping (50°–80°) (Fig. 3) with small thicknesses (1–3 m) and lengths varying from 100–200 to 1000 m.

The richest ores are reported on the northwestern flank of orebody no. 1, where ore shoot was intersected by mining works and boreholes at level 600. Trench 1 exposed a 7.4-m-thick vein swell. In addition, the largest thickness of the vein zone was intersected by drilling at the depth of 26.2 m. Based on drill intersections, silver grades vary from a few hundred to 80 567.8 g/t and gold grades are up to 655.0 g/t.

The second ore shoot is located in the central part of orebody no. 3. Silver grade in the adit is up to 17 122.4 g/t; gold grade, up to 108.4 g/t. The highest grades in drill intersections are up to 7791.4 g/t silver and up to 58.7 g/t gold.

According to exploration data, the main controlling factor in the ore mineralization has been tectonics, to which the multistage geological evolution of the deposit was closely related. Orebody formation was guided largely by northwest- and northeast trending

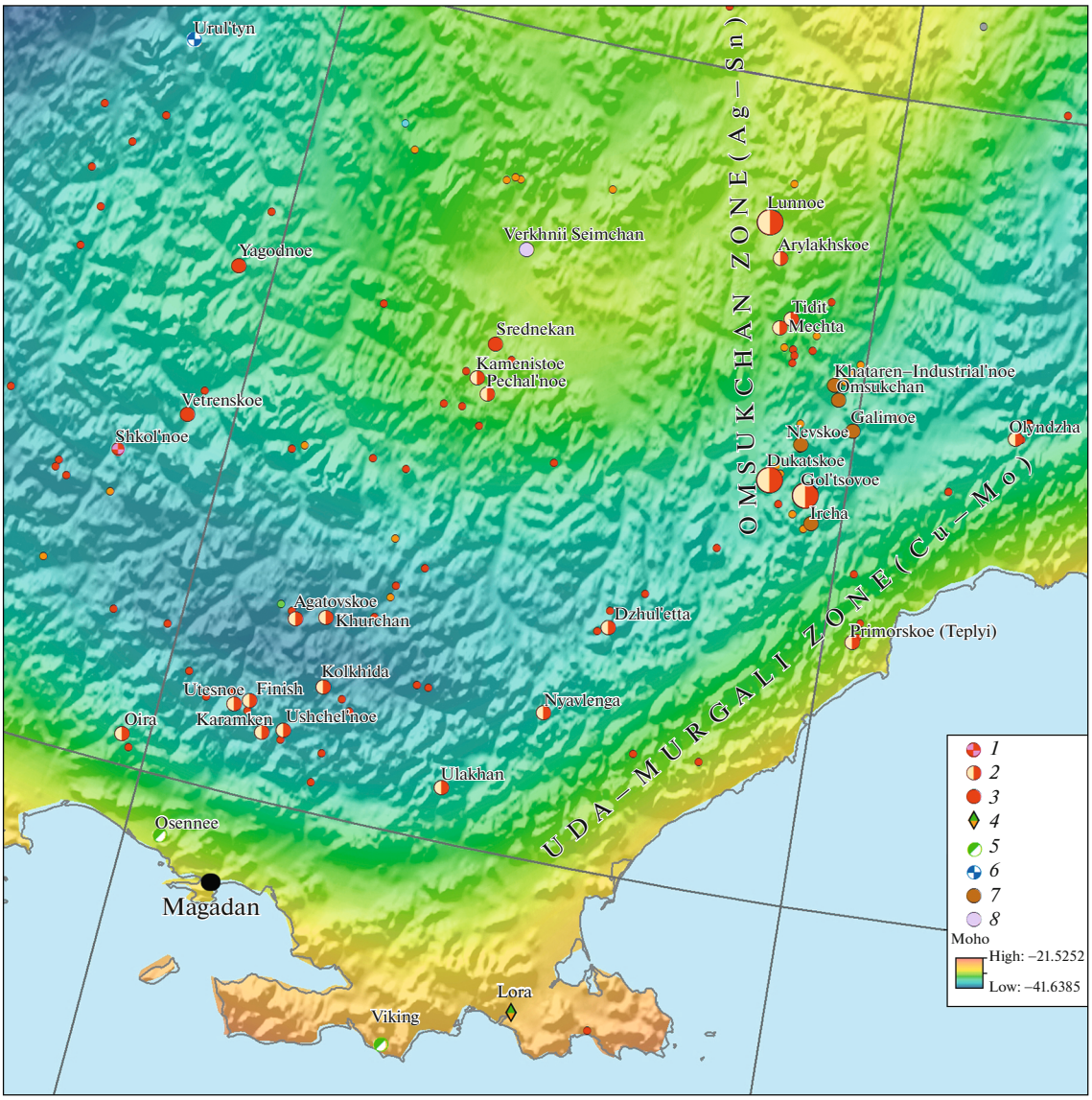

Fig. 2. Position of Primorskoe deposit relative to Uda–Murgali (Cu–Mo) and Omsukchan (Sn–Ag) metallogenic zones. Moho topography map (Panet I. et al., 2014). Mineral types of deposits: (*1*) Au–Bi related to granitic intrusions; (*2*) Au–Ag and Ag–Au epithermal (low and intermediate sulfidation); (*3*) orogenic gold; (*4*) porphyry Cu–Mo–Au; (*5*) volcanogenic massive sulfide (VMS) Cu–Pb–Zn, (*6*) Pb–Zn-stratiform in carbonate rocks; (*7*) tin; (*8*) Co-REE.

preore faults. The skeletal frame of northwest, northeast, and north–south trending fractures in the main northwest trending ore-bearing structures was formed by the beginning of the main ore emplacement stage. Changes in orebody morphology, bedding, and ore grade were determined largely by fractures of the latter two systems, which provided permeability barriers accounting for vein pinching or swelling, changes in dip angle, and the formation of vein offshoots and feather veinlet zones. As a rule, ore shoots are formed in such zones. The extremely complex fault tectonics of the ore field as the main ore-controlling factor requires further detailed studies in order to establish the optimal directions of further exploration operations at the deposit.

METASOMATITES

The location of the ore field within a volcanic dome structure accounts for the variety of zoned metasomatic alterations in host volcanic rocks—kaolin–quartz, quartz–chlorite–sericite, chlorite–

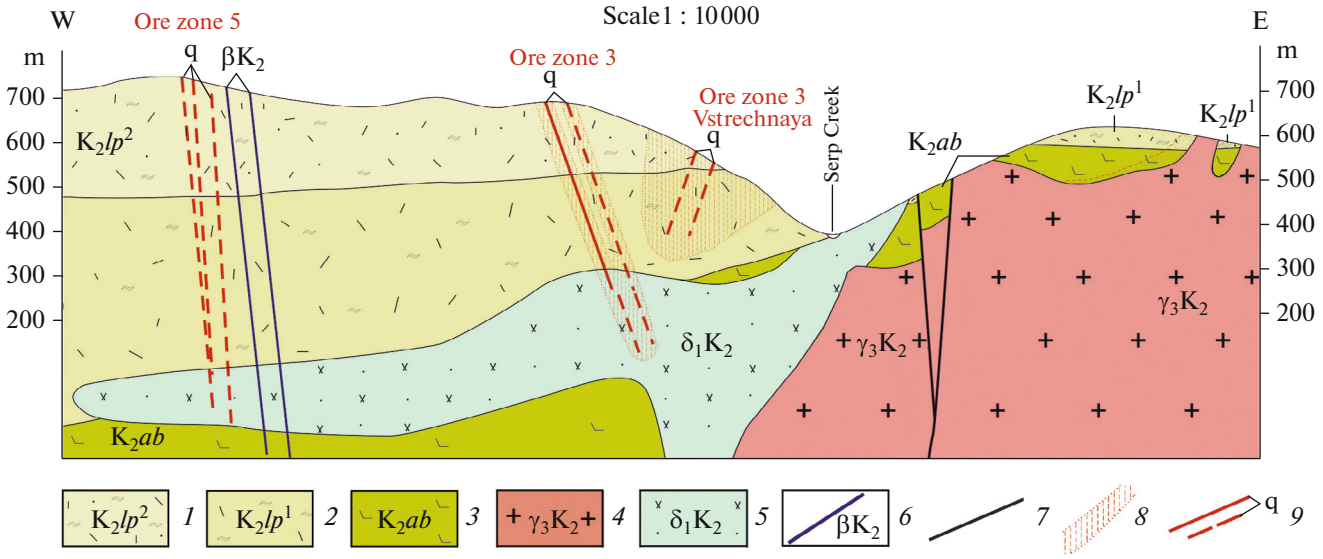

Fig. 3. Cross section of Teplyi area (W–E). Scale 1 : 10000 (after Magadangeologiya archival data). (*1*) Upper member: rhyolitic ignimbrites with andesitic tuff and tuffstone interbeds and lenses; (*2*) lower member: psammitic rhyolitic ignimbrites; (*3*) basaltic andesite series: basaltic andesites, basalts, and clastic lavas of corresponding compositions; (*4*) granites; (*5*) diorite porphyries; (*6*) basalt dykes; (*7*) faults; (*8*) illite–quartz metasomatites; (*9*) Ag–Au quartz–rhodonite veins.

epidote, and actinolite. Contact metamorphic rock—quartz–biotite–amphibole hornfels—was reported in the immediate vicinity of the surface outcrops of granitoid rocks of the Kalalaga massif.

Orebodies of the Teplyi area are located within the propylitic aureole. Low-grade and run-of-mine (ROM) ores are emplaced in propylites of the low-temperature chlorite facies; ROM ores, in medium-temperature epidote facies, and high-grade ores, in high-temperature actinolite facies (Figs. 4a–c). Exomorphic alterations in a 1- to 10-m-thick zone are represented by illite-bearing beresites, argillisites (Fig. 4d), and feldspatholites.

Chlorite–epidote metasomatites are the most widespread in the Teplyi area. Their areas of occurrence encompass virtually all stratified volcanic rocks irrespective of composition. Besides epidote and chlorite, these metasomatites indispensably contain alkali feldspar, predominantly albite, and potassium feldspar, which was sporadically encountered. In addition, elevated pyritization zones were noted in this area.

Argillisites and secondary quartzites occur in narrow zones along individual local faults or veins or in relatively wide fields in their clustering or crossing zones. Host rock alterations in exomorphic zones of orebodies 1 and 3 are manifested largely as silicification, ferrugination, and enrichment in manganese (Fig. 5). Manganese hydroxide (pyrolusite) saturated rocks usually accompany rich ores (Fig. 5).

ORE STRUCTURES

Vein mineralization structures within the deposit are massive and brecciated in monoquartz zones; massive, brecciated, and vuggy, in quartz–pyrolusite ones, and combinations of banded, colloform-banded, brecciated, and cocardelike structures were observed in quartz–pyrolusite–rhodonite veins (Figs. 6a, b). Ore-bearing zones of the veins are characterized mostly by three types of structure: colloidal, brecciated, and stockwork-type.

Ore structures of the Teplyi area are evidence for epithermal-type of mineralization. Unaltered veins display predominantly colloform-banded structures with chalcedony-like quartz and adularia and finely disseminated ore components confined to illite interlayers (Figs. 6c, 6d).

Thermometamorphic ores affected by heat from an underlying intrusion contain assemblages with widespread rhodonite, bustamite, garnet, and magnetite that display a similarity to the latest veins of the Dukat deposit (Fig. 6b). At the same time, they still retain the colloform-banded structure emphasized by black pyrolusite. Rhodonite replaces primary rhodochrosite, whose relics are occasionally preserved.

ORE MINERALOGY

The Primorskoe deposit consists of hydrothermal quartz veins emplaced in volcanic rocks. The ore mineral composition is given in Table 1. The ore consists largely of quartz (75%) with minor feldspar and micaceous clay minerals (5%), rhodonite (15%), rhodo-

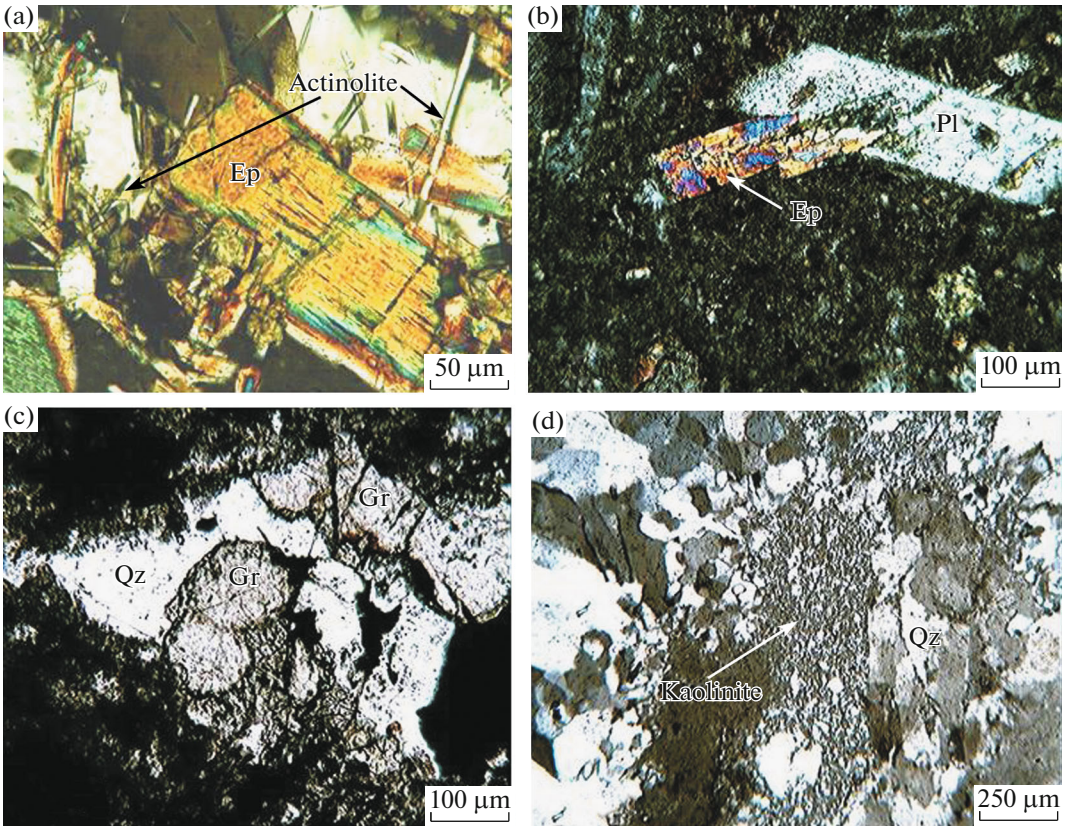

Fig. 4. Metasomatites of Teploe deposit: (a) high-temperature epidote–actinolite; (b) plagioclase corroded with epidote in andesite affected by metasomatism; (c) metasomatic (overprinted) garnet in quartzite; (d) low-temperature quartz–kaolinite metasomatites (along periphery of volcanoplutonic dome).

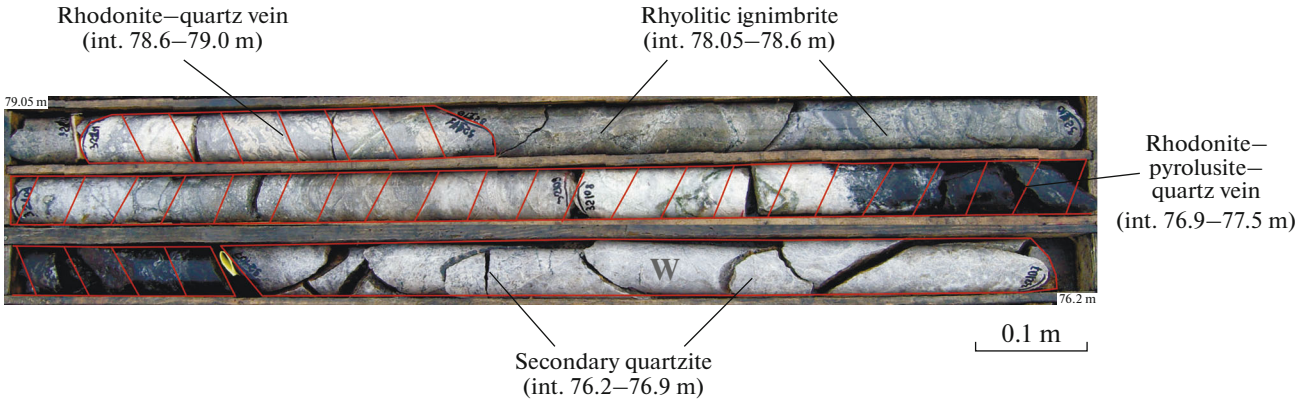

Fig. 5. Ignimbrites converted into secondary quartzites by extensive silicification at contact with ore-bearing vein. Orebody 1 (core recovered from hole 32-1, interval 76.2–79.8 m).

chrosite (<1%), Mn (5%) and Fe oxides and hydroxides, and sulfides. The content of metallic minerals (chalcopyrite, sphalerite, galena, pyrite, magnetite) is 1%. The content of Ag-bearing minerals in ores widely varies from a thousandth of a percent to 2% or more, averaging 0.05–0.06%. Total base metal sulfide content is about 1%. The predominant (up to 90%) Ag-bearing mineral in ore is acanthite, which occurs as grains varying from 0.001–0.005 to 0.3–0.6 mm across. The acanthite content in ore is about 0.1%. A small proportion of Ag is occluded in Cu–Ag sulfides or occurs as native silver. Based on rational analysis

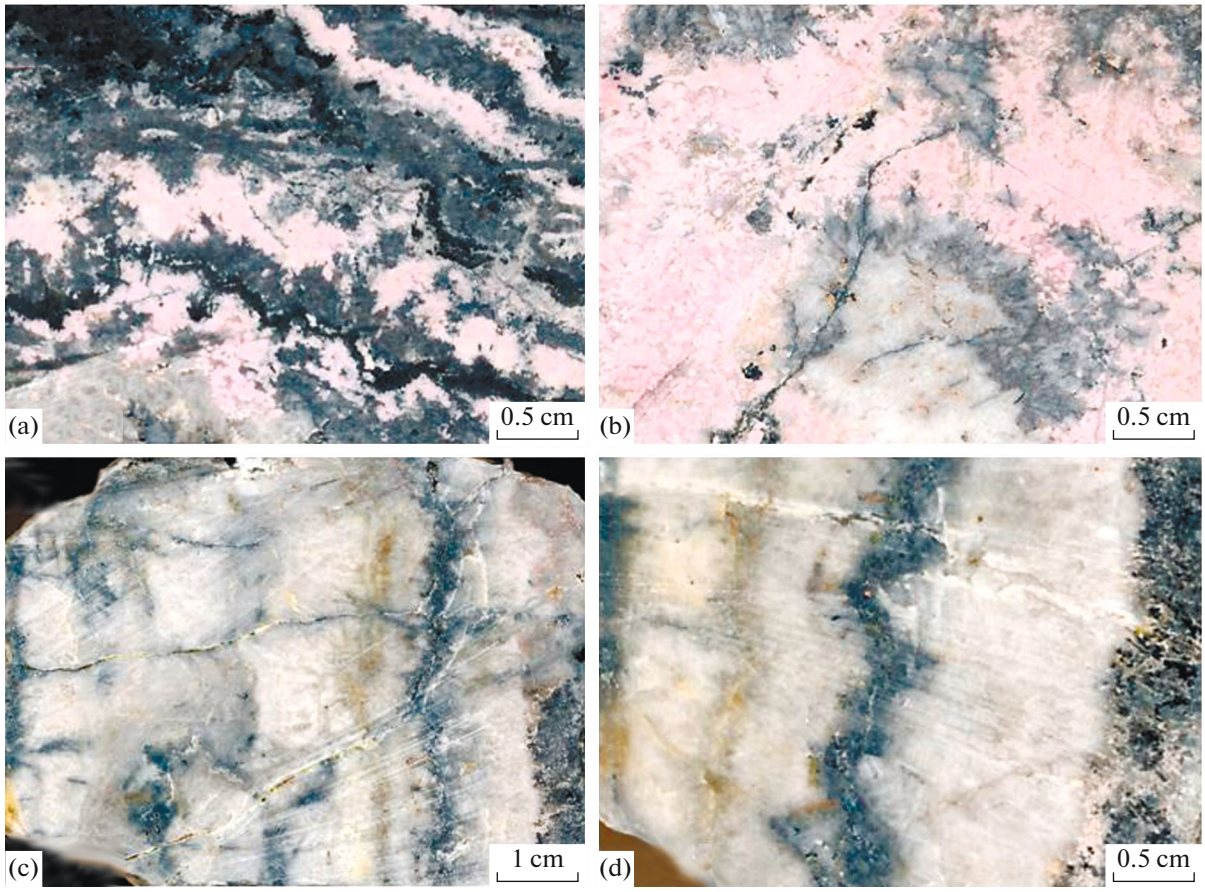

Fig. 6. Colloform–banded ore structures at Teploe deposit: (a–b) thermometamorhic quartz–rhodonite–pyrolusite ores enriched in acanthite; (c–d) quartz–chalcedony–adularia–illite ores unaffected by thermometamorphism with aggregates of finely disseminated sulfides—galena, acanthite, and polybasite—in dark stringers.

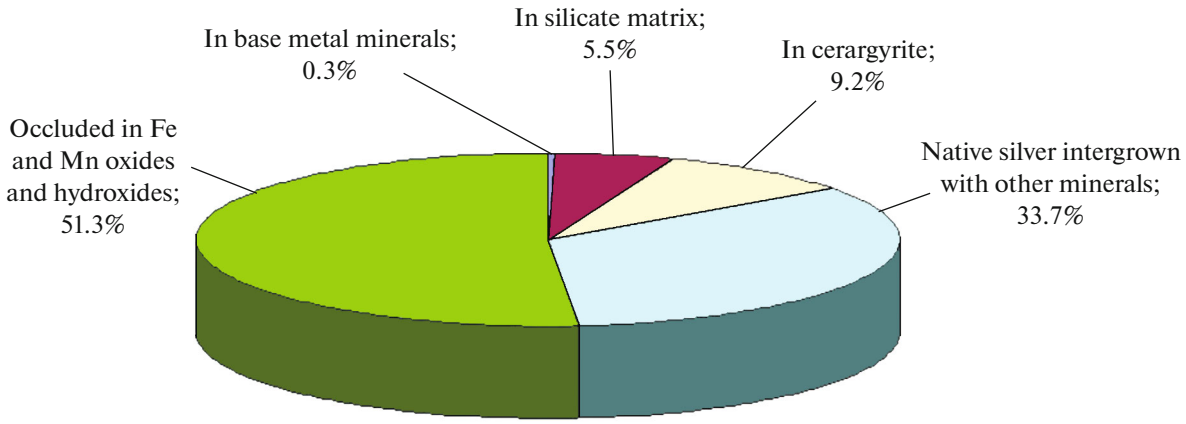

Fig. 7. Rational analysis of silver, bulk sample, Teplyi area (TsNIGRI Laboratory of Ore Concentration Technologies).

data, about half of Ag (51.3%) and a quarter of Au (23.5%) occur among Mn minerals as ultrafine inclusions and invisible mineralization (Fig. 7). A specific feature of the ore composition is abundant Mn mostly represented by three mineral species: rhodonite–bustamite, rhodochrosite, and manganese oxides.

MAJOR MINERAL CHARACTERISTICS

Gangue minerals. The overall gangue mineral content in the ore is no higher than 95–98%. In some parts of veins, gangue is >50% rhodonite and carbonate (Fig. 6b).

Table 1. Mineral composition of ores in Teplyi area as broken down by abundance group

Minerals	Major	Minor	Rare
Gangue–metasomatic	Quartz Rhodonite Epidote Chlorite Illite	Actinolite Adularia Garnet Plagioclase	Rhodochrosite Pyrophyllite Fluorite Andalusite, Wollastonite
Ore	Acanthite Galena Chalcopyrite Sphalerite Pyrolusite	Electrum Native Au Pyrite Bornite Jalpaite Lenaite Mckinstryite Polybasite Cupriferous pyrargyrite	Magnetite Hematite Stromeyerite Cupriferous uytenbogaardtite Cupriferous acanthite Matildite Native silver
Supergene	Pyrolusite Psilomelane Cerargyrite	Chalcocite Covellite Fe hydroxides	Anglesite Plattnerite PbO_2 Spertiniite $Cu(OH)_2$

Quartz is represented by three generations. *Quartz-1*, fine-grained and chalcedonic, replaces host rock together with kaolin and illite on the flanks of the deposit, remote from the central part of the volcanic dome structure. It also makes up rhythms of colloform-banded veins unaffected by strong thermal metamorphism (Figs. 6c, 6d). *Quartz-2* makes up the central parts of rhodonite–pyrolusite veins. It occurs as relatively large, up to 8 mm across, often zoned, columnar, and cockscomb aggregates. *Quartz-3* is chalcedonic up to chalcedony proper; it fills 1–4 mm veinlets that crosscut quartz-1, quartz-2, and rhodonite aggregates.

Chlorite and epidote are widespread in ore-bearing veins, but always in small amounts. These minerals are syngenetic to quartz. They occur as segregations 0.05 to 1–1.5 mm across, mostly as polycrystalline clusters, less frequently as radial fibrous aggregates. Epidote distinctly corrodes plagioclase insets. Chlorite occurs as scaly aggregates up to 5 mm across. It is similar to prochlorite in optical characteristics.

Actinolite is reported as a secondary mineral of high-temperature metasomatites in the above-intrusion zone of the volcano-plutonic dome together with epidote (Fig. 4a), but sometimes it penetrates quartz in high-temperature veins of the second stage.

Rhodonite makes up bands up to 2.5 cm in thickness and lenses in veins of the second phase of mineralization, oriented roughly parallel to contacts. Thin-section microscopy data suggest that rhodonite crystallizes almost synchronously with gangue quartz. Quartz and rhodonite display mutual intergrowths, and rhodonite is replaced by psilomelane and pyrolusite as a result of oxidation. Veins often contain rhodonite spherulites and finely colloform structures consisting of columnar crystalline quartz alternating with fine-crystalline rhodonite; both rhodonite and quartz are found in the cores, but the latter is frequent. Rhodonite also occurs as fine impregnation or irregularly shaped polycrystalline concretions in fine and extra-fine-grained quartz. According to X-ray spectral spot analysis data, rhodonite contains fine (0.2–0.6 mm) interstitial acanthite disseminations and fine native Ag stringers.

Rhodochrosite is the latest gangue mineral. It was observed as relics in quartz–rhodonite–pyrolusite veins that make up pocketlike aggregates up to 3–5 mm across; it also fills small vugs and fractures. It grows into hypogene pyrolusite and is replaced by supergene psilomelane. The largest amount of this mineral (about 50% of the gangue) was reported on the southern flank of orebody no. 3. Rhodochrosite is rapidly leached in a supergene environment.

Garnet in minute amounts is ubiquitous in veins. Its concentration is 0.01% with some minor exceptions. Segregations vary in size from submicroscopic to 2–3 mm across (Fig. 4c). Garnet mineralization is typically disseminated or stockwork-type. Two garnet generations have been identified. Early-generation garnets characterized by anomalous birefringence and very sparse twins occur as small xenomorphs frequently arranged in polyaggregate clusters. These garnets are associated with rhodonite, feldspar, and magnetite. Second-generation garnets occur as well-developed transparent rhombic dodecahedral crystals filling fractures and solution cavities. The crystals are up to 1.5–2.0 mm across. These garnets are associated with epidote, actinolite, and quartz.

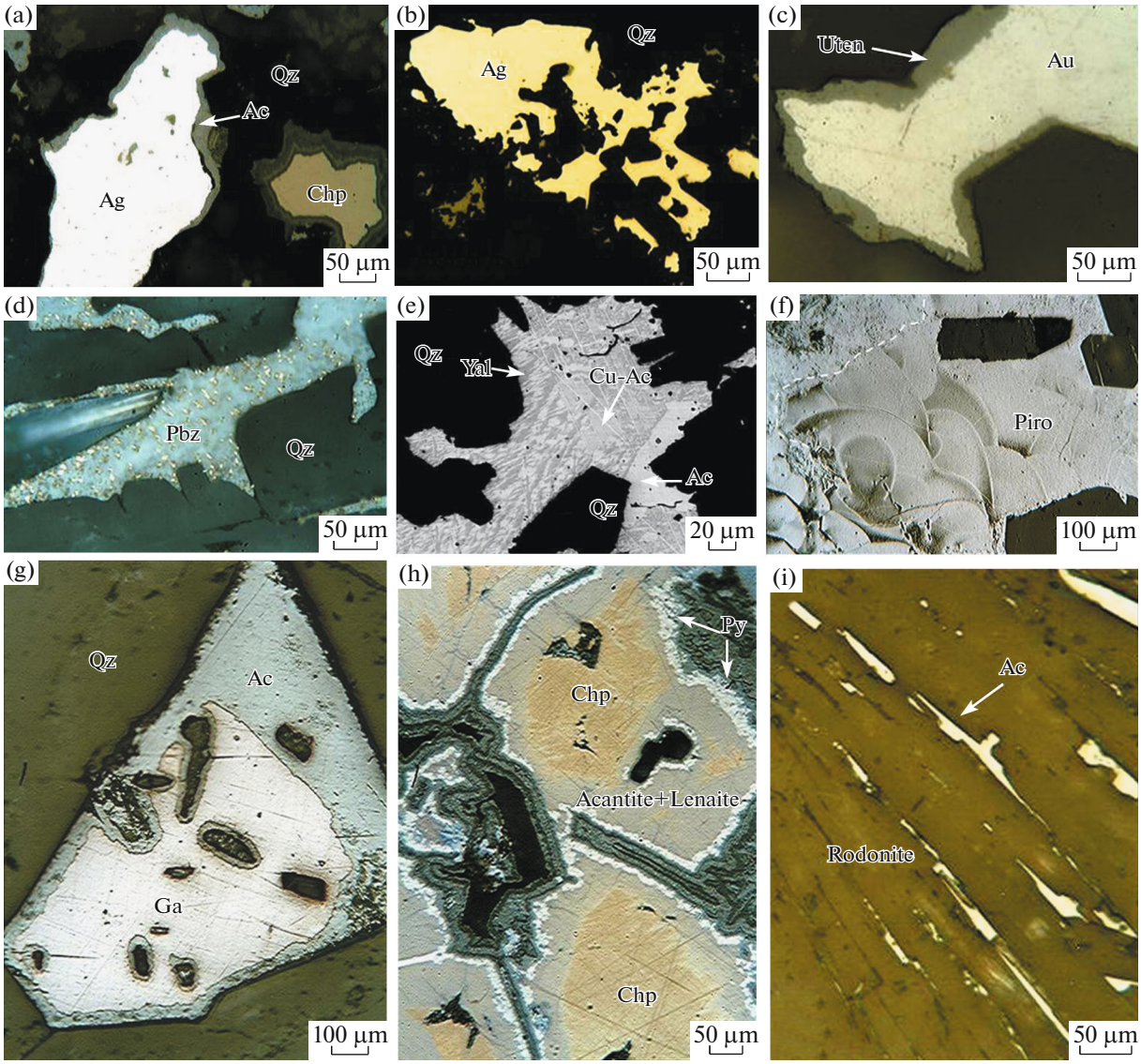

Fig. 8. Ore mineral segregations in ores of Teplyi area: (a) native silver with cupriferous acanthite rim; (b) native gold in quartz–adularia aggregate; (c) uytenbogaardtite rim on electrum; (d) polybasite with light etching structure; (e) exsolution structure: acanthite–cupriferous acanthite–jalpaite (electron-beam image); (f) hypogene pyrolusite intergrown with quartz and feldspar; (g) acanthite rim on galena; (h) zoned acanthite, lenaite, and pyrite deposited on chalcopyrite; (i) acanthite segregation in rhodonite.

Adularia is classified as a minor gangue mineral within the deposit. It occurs in tight intergrowth with quartz-1 in colloform-banded veins of the early mineralization stage. Adularia crystals are no more than 0.5 mm across.

Illite replaces host rock and occurs as rhythms (1–3 mm) in colloform-banded veins. Fine ore mineral dissemination is often associated with illite bands.

Ore minerals occur as disseminations, bands, and clusters confined to colloform zone boundaries (Figs. 6c, d), and brecciated vein fragments. The most favorable for ore emplacement are quartz in the immediate vicinity of massive rhodonite ores; quartz fragments occluded in rhodonite or quartz with finely disseminated rhodonite; contacts of fine-crystalline and coarse-crystalline quartz, and heterogeneous speckled quartz. The main valuable component of the ores—Ag—occurs as native metal or in sulfides usually confined to Mn mineralization areas. Rational analysis data of Ag are shown in the diagram in Fig. 7. Ore mineral compositions in the Teplyi area are summarized in Tables 2 and 3.

Native Ag is found in ores as small round segregations up to 0.8 mm across with acanthite and jalpaite rims (Fig. 8a). Microprobe analysis data always contain excessive sums, but no impurities in silver were

Table 2. Chemical composition of ore minerals of Teploe deposit based on X-ray spectral microanalysis data (wt %)

Analysis no	Element concentrations, wt %					Total
	Cu	**Fe**	**S**	**Ag**	**Sb**	
Acanthite						
1	0.8		12.91	86.18		99.89
2			11.6	87.53		99.14
3	0.59		9.41	91.09		101.09
Chalcopyrite						
1	34.03	29.04	34.55			97.62
2	30.4	27.41	32.33	8.68		98.82
3	28.8	28.9	33.75	10.29		101.74
Polybasite						
	Cu	**Sb**	**S**	**Ag**	**Se**	
1	2.17	5.98	13.19	75.24	1.65	98.24
2	3.02	7.48	12.95	76.01	0.65	100.11
3	2.87	6.03	13.12	75.22	1.14	98.65
Cupriferous pyrargyrite						
1	4.04	19.08	17.51	57.01		97.64
2	3.93	18.55	17.03	56.20		95.71
Lenaite						
	Cu	**Ag**	**S**	**Fe**	**Zn**	
1	1.18	48.29	26.23	22.05		97.76
2		48.83	28.45	25.08		102.37
3		49.07	28.66	25.12		102.85
Galena						
	Cu	**Ag**	**S**	**Pb**	**Bi**	
1			12.89	85.95		98.85
2			13.28	86.91	0.31	100.50
3			13.03	87.52	0.45	101.00
Matildite						
1		27.81	17.18	1.22	54.17	100.38
2		26.69	17.23		56.01	99.93
Sphalerite						
	Cu	**Ag**	**S**	**Fe**	**Zn**	
1	0.41	1.04	32.76	1.04	65.06	99.28
2	0.46		33.05		65.93	99.93
3			33.58		67.21	100.8
Cupriferous uytenbogaardtite						
	Cu	**Fe**	**S**	**Ag**	**Au**	
1	5.62		10.52	61.48	20.38	98.95
2	5.95		10.97	60.05	22.03	99.01
Electrum						
1				50.94	49.06	100.00
2				51.00	48.90	99.90
3				48.55	50.42	98.97

Camebax X-ray microanalyzer equipped with an INCA add-on device, analysts E.M. Goryacheva and T.V. Subbotnikova (SVKNII FEB RAS) and I.A. Bryzgalov (MSU). Calibration curves, standards: TeL_a, Bi_2Te_y. Bi_2S_3 (Bi, 52.2; 81.3); Cu K_a, $CuFeS_2$ (34.5, Cu; 30.5, Fe; 34.5, S); Fe$K_\acute{\alpha}$, FeS_2 (46.55, Fe); SeK_a, PbSe (27.6, Se); Ag$L_\acute{\alpha}$, alloys of various compositions.

Table 3. Chemical compositions of jalpaite–mckinstryite–stromeyerite mineral series

	Element concentrations, wt %				Formula coefficients		
Seq.	**Ag**	**S**	**Cu**	**Total**	**Ag**	**S**	**Cu**
Jalpaite Ag_3CuS_2							
1	74.97	8.75	15.43	99.15	3.44	1.35	1.2
2	71.21	10.11	17.92	99.24	3.15	1.5	1.35
3	72.62	11.19	16.48	100.29	3.15	1.63	1.21
4	71.09	10.64	18.67	100.4	3.08	1.55	1.37
5	70.45	11.24	18.07	99.76	3.04	1.63	1.32
Mckinstryite $(Ag, Cu)_2 S$							
1	57.83	12.85	27.37	98.05	1.18	0.88	0.94
2	67.67	12.43	20.85	100.95	1.40	0.87	0.73
3	68.38	11.33	19.24	98.95	1.47	0.82	0.70
4	60.12	13.1	27.33	100.55	1.20	0.88	0.92
5	63.22	11.17	23.97	98.36	1.34	0.80	0.86
6	59.21	17.31	23.13	99.65	1.13	1.11	0.75
7	54.04	17.53	27.53	99.10	1.01	1.11	0.88
8	58.29	16.81	25.51	100.61	1.11	1.07	0.82
Stromeyerite AgCuS							
1	52.83	15.22	31.2	98.25	1.01	0.98	1.01
2	52.76	15.13	33.33	101.22	0.99	0.95	1.06
3	55.91	14.95	29.36	100.22	1.07	0.97	0.96
4	56.22	13.18	29.09	98.49	1.12	0.89	0.99
5	58.53	12.15	28.36	99.04	1.19	0.83	0.98
6	57.10	15.34	28.53	100.97	1.09	0.99	0.92
7	53.78	15.85	30.80	100.43	1.01	1	0.98
8	52.90	18.34	28.8	100.04	0.97	1.13	0.9

Camebax X-ray microanalyzer, analysts: E.M. Goryacheva and T.V. Subbotnikova (SVKNII FEB RAS) and I.A. Bryzgalov, MSU). Calibration curves, standards: TeL_a, Bi_2Te_y, Bi_2S_3 (Bi, 52.2; 81.3); CuK_a, $CuFeS_2$ (34.5, Cu; 30.5, Fe; 34.5, S); FeK_a, FeS_2 (46.55, Fe); SeK_a, PbSe (27.6, Se); AgL_a, alloys of various compositions.

detected, which is more typical of supergene mineralization.

Native Au is low-fineness (443–616‰). Thirty-one fineness measurements were taken by microprobe (Fig. 9a). Segregations are 0.1–1.1 mm across. They are represented by cloddy grains with numerous branches, scales, single elongate crystals, and bundle-shaped or linear crystal clusters. Ag overgrowth at grain peripheries was noted. Native gold is intergrown with quartz, adularia, and rhodonite (Fig. 8b). Fortunately for concentration purposes, it is never intergrown with sulfides. When found in surface mining workings, it is rimmed with Cu-uytenbogaardtite (Fig. 8c). The fineness histogram displays a lognormal distribution with a peak in the interval of 450–500‰ (Fig. 9a). Two native Ag fineness measurements are also included here. The average fineness (excluding native Ag) is 502.89‰.

Galena occurs as interstitial segregations (0.1–2.5 mm across) characterized by a highly nonuniform distribution. Its composition corresponds to stoichiometric (Table 2). It is intergrown with acanthite, sphalerite, and chalcopyrite. Acanthite forms thin (0.008–0.01 m) rims around galena grains (Fig. 8g). Galena is closely associated with sphalerite, and their intergrowth patterns attest to their synchronous formation.

Chalcopyrite is among the most widespread ore minerals. It occurs as fine disseminations (occasionally as stringers) in quartz, often in association with magnetite and Ag sulfides, and as interstitial segregations in quartz and rhodonite. Its inclusions are frequent in galena, and disseminated chalcopyrite emulsion in sphalerite is widespread. Chalcopyrite inter-

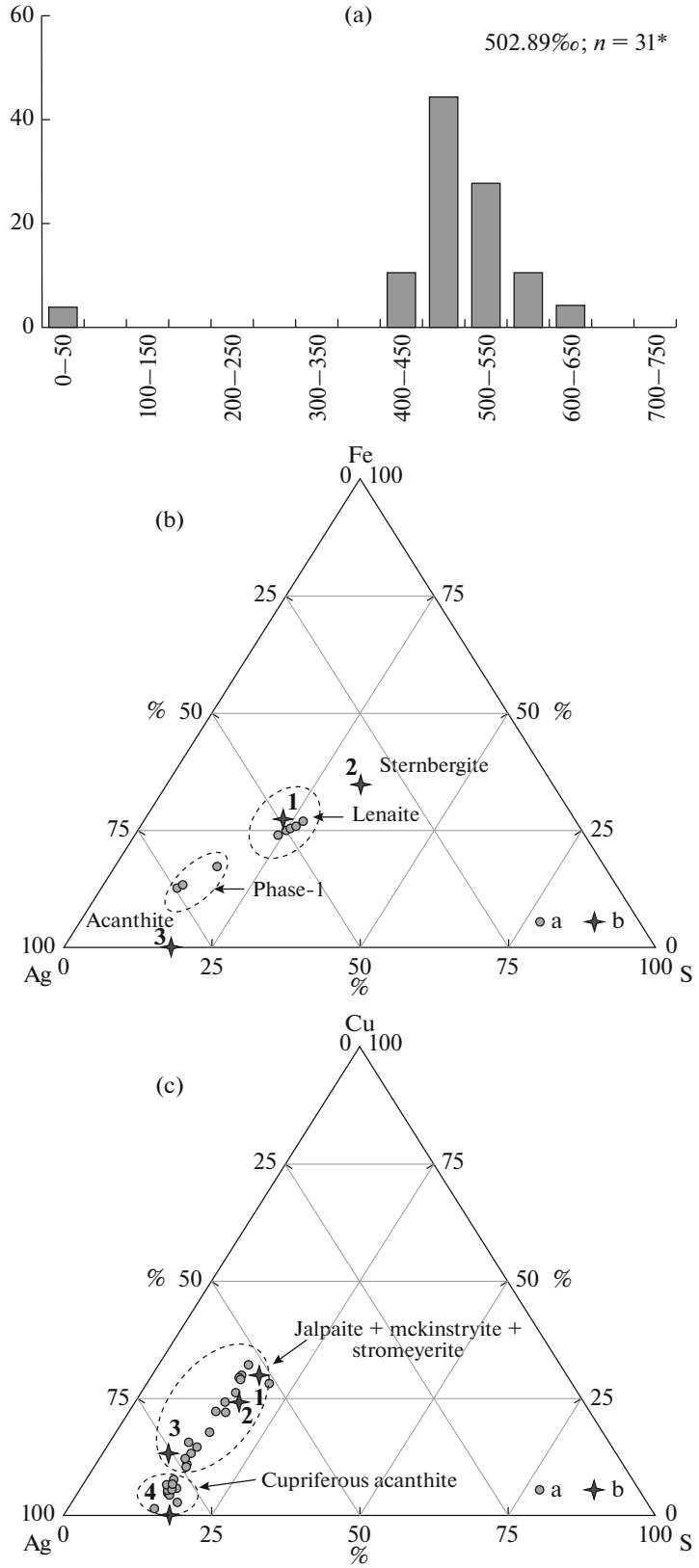

Fig. 9. Distribution of gold fineness (a) and nonstoichiometric mineral phases in Fe–Ag (b) and Cu–Ag (c) massive sulfide ores of Teplyi area. (a) Histogram of native gold fineness in ores of Teploe deposit: fineness intervals, ‰, along *X* axis, and frequency, %, along *Y* axis; (*n*) number of analyses; 502.89‰, average fineness; (b) (Ag–Fe–S) phase diagram: (a) phases of Teplyi area; (b) theoretical compositions: (*1*) lenaite, (*2*) sternbergite, (*3*) acanthite; (c) (Ag–Cu–S) phase diagram: (a) phases of Teplyi area; (b) theoretical compositions: (*1*) jalpaite, (*2*) mckinstryite, (*3*) stromeyerite, (*4*) acanthite.

growth with acanthite leads to the formation of lenaite (Ag-bearing equivalent of chalcopyrite, Table 2), which forms zoned overgrowths on chalcopyrite grains (Fig. 8h). Chalcopyrite often contains 1–10 wt % Ag as an impurity (Table 2) and is often replaced by bornite, covellite, and chalcocite.

Lenaite ($AgFeS_2$) was observed inside chalcopyrite–acanthite intergrowths, where it fills interstices (Fig. 8h). Mineral composition is stoichiometric (Table 2), but there are phases presumably consisting of an acanthite–lenaite mixture, shown in diagram as phase-1 (Fig. 9b).

Sphalerite occurs as xenomorphic crystals (0.2–1.3 mm across) and as separate grains both in quartz and its interstices. Weakly cataclastic sphalerite and sphalerite overgrown by acanthite were noted. In terms of composition, sphalerite is iron-free and depleted in iron (<1.02 wt % Fe) (Table 2). It is often covered by a thin (0.006–0.008 mm) acanthite rim. Keeping a polished section in the open for a long time (2–3 months) leads to the development of newly formed acanthite (its penetration through a carbon coating was noted).

Acanthite occurs as tight intergrowths (Cu-acanthite–jalpaite–mckinstryite–stromeyerite) in quartz and rhodonite interstices (Figs. 8a, e, g, and i). Segregation sizes widely vary from submicroscopic to 3–4 mm, the predominant size being 0.1–0.3 mm; locally, 0.01–0.1 mm. Acanthite crystal clusters are sporadically found in solution cavities. Acanthite distribution in veins is extremely nonuniform, accounting for bonanza grades in some samples. Late mineral assemblages display exsolution structures (Fig. 8e) with a wide range of Cu–Ag sulfide compositions (Table 3, Fig. 9c).

Pyrite is a rare ore mineral. It is found predominantly in quartz–sericite metasomatites and on the flanks of orebodies. It occurs as xenomorphic crystals often split into elongate blocks by overprinted rhodonite. These segregations are up to 1 mm in size. Late-phase microcrystalline pyrite deposited as a corrosion rim on the flanks of lenaite and acanthite crystals that replace chalcopyrite (Fig. 8h) was also observed.

Polybasite is a rare mineral; it was encountered on the western flank of trench 1, where it fills interstices in quartz as segregations 0.5–1.1 mm across. The mineral is unstable during optical investigations: it excretes large drops of Ag when exposed to light etching (Fig. 8d). Polybasite was found to contain up to 1.65 wt % Se as an impurity (Table 2).

Cu-pyrargyrite was encountered in intergrowth with chalcocite, where it makes up thin rims no thicker than 0.3 mm. Its composition deviates from stoichiometry owing to an Sb deficiency (Table 2).

Bornite is intergrown with spongy chalcocite–covellite aggregate in the form of small pinkish gray segregations no larger than 0.5 mm across. Its hypogene or supergene origin remains questionable, because the oxidation zone is incipient and the amount of copper minerals in ores is notably large.

Matildite is a rare mineral encountered in samples from the dumps of adit 1. It is tightly intergrown with galena and anisotropic. The mineral was identified by microprobe (Table 2).

Cupriferous uytenbogaardtite (5–6 wt % Cu) is ubiquitous as rims on electrum. It was identified by microprobe (Table 2).

Magnetite is reported as intergrown with rhodonite and pyrolusite in the gangue. Its content is up to 20–35% (up to 90–95%) of the heavy crop after panning. Magnetite occurs as aggregates of fine (0.2–0.5 mm) subeuhedral grains. Two magnetite generations have been recognized. The early generation is characterized by complex morphology, abundant inclusions and cavities, and the presence of exsolution structures. It contains quartz, chalcopyrite, pyrite, galena, acanthite, native Fe, chlorite, and native Ag inclusions. Late generation magnetite is less frequent and consists of well-developed crystals and their clusters, often zoned. Other mineral inclusions in this magnetite are rare.

Pyrolusite—presumably, both hypogene and supergene—is widespread. It occurs as large aggregates up to 10 cm across, often together with psilomelane sinter (Fig. 8f).

The paragenetic sequence in mineral formation based on interrelationships and structural positions of minerals and mineral assemblages has been worked out (Table 4). Three mineralization stages were recognized: *volcanogenic stage I*, subdivided into two substages, quartz–adularia–illite–sulfide–sulfosalt substage with native **Au** and quartz–carbonate (manganocalcite–rhodochrosite) substage; *plutonogenic stage II*, conventionally subdivided into two substages, superimposed high-temperature metasomatism—epidote–rhodonite–bustamite–pyrolusite with garnet—and a substage of redeposited ore minerals—quartz–sulfide with acanthite, minerals of Ag–Cu–S and Ag–Fe–S groups, and native **Au** and **Ag**; and *supergene stage III*—predominantly Fe and Mn hydroxides with a noticeable amount of chalcocite.

RESULTS OF FLUID INCLUSION STUDIES

Six samples were collected from orebodies no. 1 and 3 to study quartz–rhodonite vein emplacement conditions in the Teplyi area. Thirty-five individual fluid inclusions (FIs) in second-generation quartz were studied by thermobarogeochemistry methods. The results of FI studies are summarized in Table 5.

At room temperature, FIs are two-phase, gas–liquid (L-type) fluids consisting of an aqueous–salt solution (F = 0.3–0.9) (Fig. 10). FIs are isometric, sometimes round, nonuniformly distributed, and occur predominantly along growth zones, sometimes in groups. They are 1–15 μm, predominantly 1–3 μm,

Table 4. Paragenetic sequence of mineralization at Teploe deposit

MINERAL	Stage				
	VOLCANOGENIC		PLUTONOGENIC		SUPERGENE
	Substage				
	Quartz–adularia–illite–sulfide–sulfosalt + Au	Quartz–carbonate (essentially rhodochrosite)	Epidote–rhodonite–bustamite–pyrolusite with garnet	Quartz–sulfide with acanthite and Ag–Cu–S and Ag–Fe–S + Ag groups of minerals	Essentially pyrolusite and chalcocite–covellite
Epidote					
Actinolite					
Quartz + chalcedony					
Rhodonite					
Chlorite					
Illite					
Adularia					
Manganocalcite					
Rhodochrosite					
Magnetite					
Pyrite					
Marcasite					
Hematite					
Galena					
Chalcopyrite					
Bornite					
Sphalerite					
Polybasite					
Lenaite					
Acanthite					
Jalpaite					
Mckinstryite					
Stromeyerite					
Uytenbogaardtite					
Matildite					
Electrum					
Native Au					
Native Ag					
Pyrolusite					
Psilomelane					
Cerargyrite					
Chalcocite					
Fe hydroxides					
Anglesite					
Plattnerite					
Spertiniite					

in diameter. Primary and primary–secondary FIs 3–15 μm across were collected for cryometric and thermometric studies.

FIs homogenize at temperatures ranging from 365 to 120°C, 253°C on average (Table 5, Fig. 11). The homogenization temperatures display a bimodal distribution: most cases of FI homogenization fall into two closely spaced temperature intervals of 297–285 and 260–220°C (Fig. 11); interestingly, fluid salinities dropped considerably during both periods. Cryometric studies demonstrated that fluid salinities vary from 3.39 to 0.35 wt % NaCl eq. as estimated from the temperatures at which the last ice crystal melted (Table 5). Eutectic temperatures (T_e) ranging from –35 to –15°C

Table 5. Results of thermo- and cryometric studies of individual fluid inclusions in ore-bearing quartz of Teplyi area

Sample no.	Phase transition temperatures, °C			Estimates:	
	Th	Te	$Tm_{(ice)}$	salinity, wt % NaCl eq.	total fluid density, g/cm^3
Tep-1-15	338...275	–25...–24	–0.5...–0.2	0.88...0.35	0.61
	273...260	–23.3	–2...–1.1	3.39...1.91	0.68
	230...220	–28	–1.1...–0.3	1.91...0.53	0.8
	207...199	abs	–1.7...–1	2.9...1.74	0.8
	185...120	–24	–0.5...–0.2	0.88...0.35	0.9
Tep-2-15	326...254	–24...–23	–1.8...–0.8	3.06...1.4	0.6
	252...220	abs	–0.5...–0.3	0.88...0.53	0.8
T-2-2	347...320	–23...–15	–1...–0.6	1.74...1.05	0.6
	290...233	abs	–0.4	0.7	0.8
	180	–19	–1.2	2.07	0.9
178-1	365	–35	–0.3	0.53	0.6
PT-3	285	–13	–0.2	0.35	0.6
M-3-1	255	–15	–1	1.74	0.8

Each row in table characterizes a group of inclusions (three to five) with similar PTX parameters present in one sample; "abs," phase transition is absent or indistinct.

Table 6. Chemical composition of ores (wt %) in Teplyi area of Primorskoe deposit

Sample no.	SiO_2	TiO_2	Al_2O_3	Fe_2O_3 total	MnO	MgO	CaO	Na_2O	K_2O	P_2O_5	S total	Σ
T-2-2	82.22	0.01	1.24	1.32	10.95	0.43	3.39	0.14	0.17	0.02	0.05	99.94
K-19-2	76.19	0.01	0.39	0.62	18.39	0.24	3.95	0.09	0.05	<0.02	0.03	99.96
178-2	83.94	0.09	6.55	0.38	2.99	0.33	2.51	0.49	2.40	0.04	0.06	99.79
178-3*	96.62	0.04	1.05	0.29	0.81	0.16	0.43	0.12	0.12	0.03	0.15	99.82
Sht. 4	64.94	0.94	11.58	5.94	1.78	3.21	6.42	3.32	1.40	0.35	0.04	99.92
M-3-1	82.51	0.01	0.92	1.06	12.00	0.28	2.76	0.14	0.18	0.02	0.02	99.91
177-1*	76.02	0.02	0.42	0.41	14.05	0.43	8.41	0.09	0.05	0.03	0.03	99.96
2925	85.92	0.10	2.73	1.41	6.78	0.39	1.81	0.35	0.27	0.06	0.03	99.86
31205	87.15	0.02	3.34	0.75	3.99	1.19	1.93	0.31	1.02	0.02	0.08	99.81
312	64.30	0.02	11.17	2.59	12.62	0.95	0.68	1.35	5.08	0.03	0.08	98.87
Avg	79.98	0.12	3.93	1.47	8.43	0.76	3.22	0.64	1.07	0.06	0.05	99.79
BS	80.4	0.08	3.68	2.1	7.48	n.d.	1.84	0.26	0.84	0.03	0.05	96.76

Avg, average concentration; BS, bulk sample X-ray fluorescence (silicate) analysis, IGEM RAS laboratory, analyst A.I. Yakushev; chemical analysis, TsNIGRI laboratory.

attest to the prevalence of Na chlorides in the fluids Aqueous extract analysis (on five samples) data confirm the prevalence of Na in fluids and suggest, in addition, the presence of K in fluids in approximately equal concentrations with an average Na/K = 1. Moreover, the fluids contain Ca, Fe, and Mg. The average (Na + K)/(Ca + Mg + Fe) = 16. CO_2, N_2, and CH_4 were not detected by Raman spectroscopy in the gas phase of FIs in a quartz sample from quartz–rhodonite ores of the Teplyi area.

The synore stage pressure estimates do not exceed 100 bar, which is more typical of open ore systems formed in open fractures near the surface, where the total pressure is controlled by the vapor pressure and

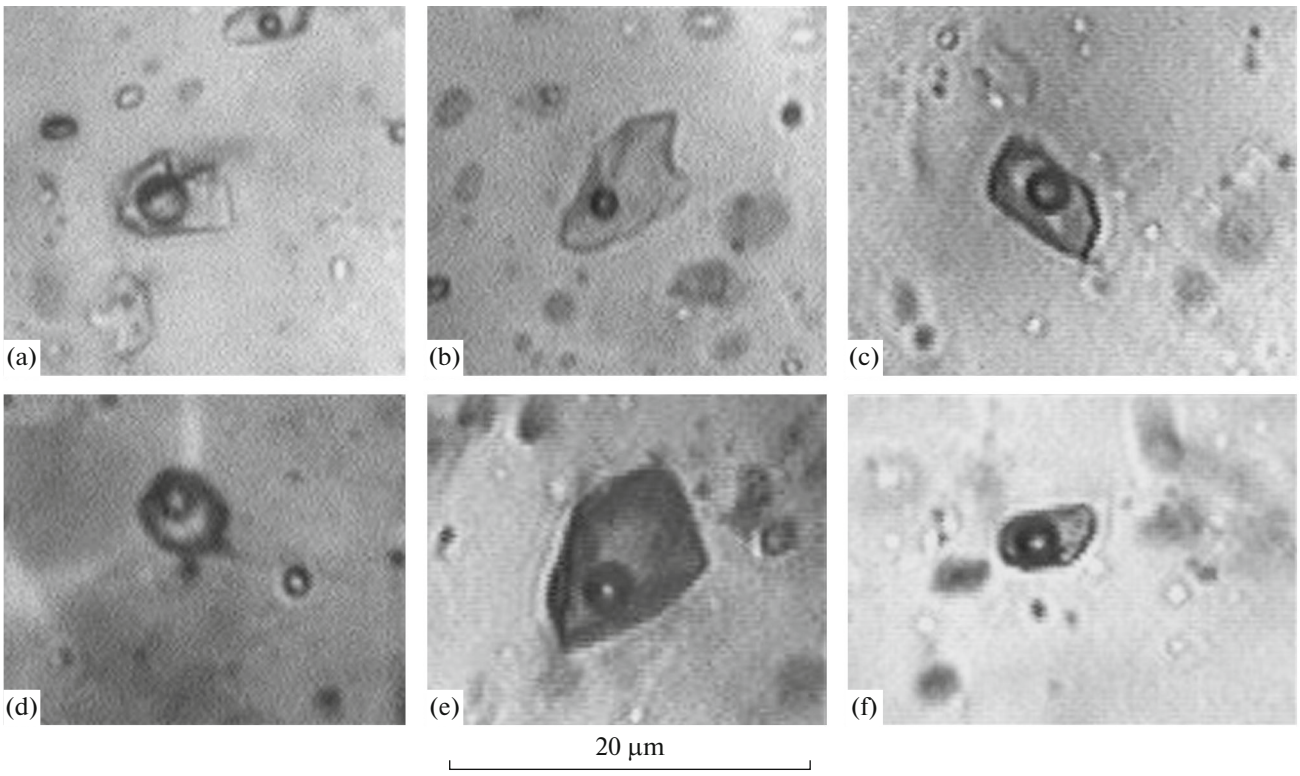

Fig. 10. Gas–liquid fluid inclusions (L-type) in ore-bearing quartz of Teplyi area. (a) Th = 338°C, Te = –25°C, salinity = 0.88 wt % NaCl eq.; (b) Th = 123°C, salinity = 0.88 wt % NaCl eq.; (c) Th = 185°C, Te = –24°C, salinity = 0.35 wt % NaCl eq.; (d) Th = 278°C, Te = –23.3°C, salinity = 3.39 wt % NaCl eq.; (e) Th = 290°C, Te = –23.7°C, salinity = 0.35 wt % NaCl eq.; (f) Th = 326°C, salinity = 3.06 wt % NaCl eq.

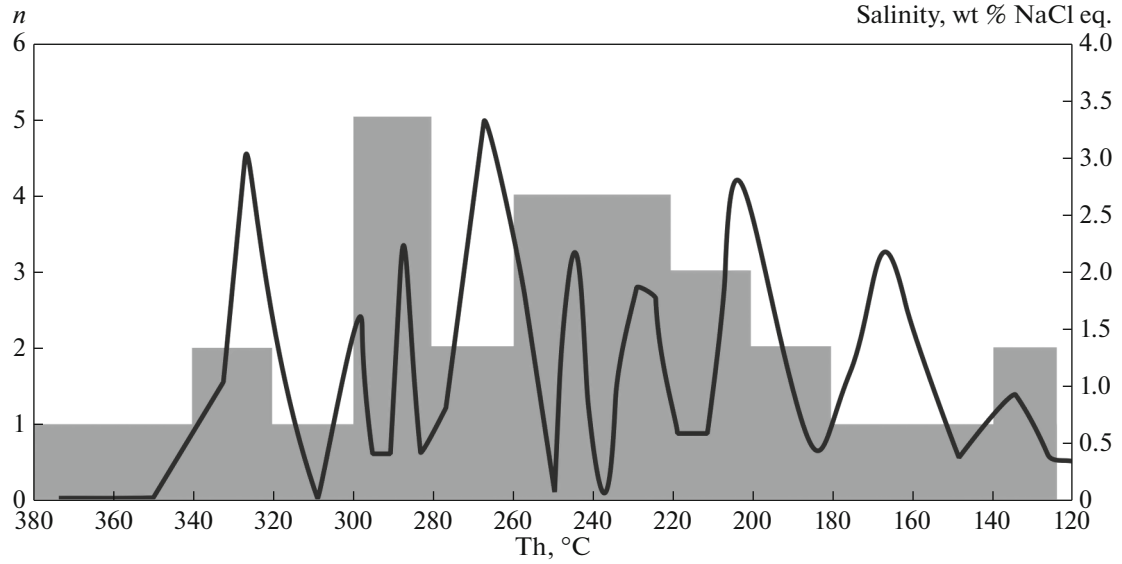

Fig. 11. Histogram of homogenization temperature and salinity of studied fluid inclusions in quartz samples from orebodies 1 and 3 in Teplyi area.

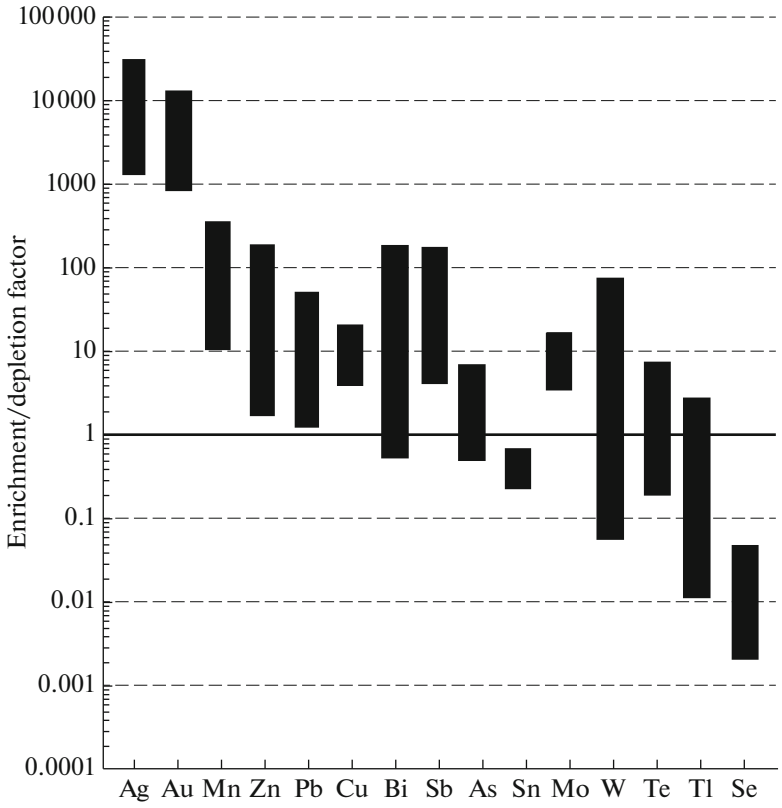

Fig. 12. Geochemical data for ten ore samples from Teplyi area.

ore mineralization takes place on the background of mineralized hydrothermal fluid boiling and mixing with vadose water (Prokof'ev, 2000). The formation depth has been estimated at 1.3–1.5 km in the case of only hydrostatic pressure in the open system (Prokof'ev and Pek, 2015).

ORE GEOCHEMISTRY

The studied ores of the Teplyi area are composed predominantly of SiO_2 (64.3–96.62%) with appreciable concentrations of MnO (0.81–18.39), Al_2O_3 (0.92–11.58), CaO (0.43–8.41), Fe_2O_3 (0.29–5.94), K_2O (0.05–5.08), and MgO (0.16–3.21) (Table 6). This suggests that orebodies consist largely of quartz and manganese minerals with minor adularia, carbonates, and illite. The ores are characterized by low and very low percentages of Na_2O, TiO_2, and P_2O_5 (Table 6). As is clear from Table 6, the sulfide content in the studied ores is very low (average S_{total} = 0.05). Low-sulfide mineralization with low Cu, Pb, and Zn concentrations (Table 7) are not typical of epithermal Ag–Au deposits (Struzhkov and Konstantinov, 2005). At the same time, the Au/Ag ratio in ores of the Teplyi area varies from 0.003 to 0.02, 0.005 on average (Table 7), typical of epithermal Ag–Au deposits (Struzhkov and Konstantinov, 2005). The convergence of our data with bulk sample analysis data is noteworthy (Table 6).

The element concentrations in ores of the Teplyi area are summarized in Table 7 and Fig. 12. In the spider plot in Fig. 12, they are normalized to average upper-crustal values (Teilor and Mak-Lennan, 1988). The chondrite-normalized REE spectra of the studied ores are shown in Fig. 13.

Ores of the Teplyi area are enriched in a fairly wide range of elements (Ag, Au, Mn, Cd, Bi, Sb, Zn, Pb, W, Cu, In, and As) (Table 7, Fig. 12), as compared with average upper-crustal values (Teilor and Mak-Lennan, 1988). The enrichment factors vary from severalfold (Cu, In, As) to tenfold (Bi, Sb, Zn, Pb, W), hundredfold (Mn, Cd), thousandfold (Au), and ten-thousand-fold (Ag) (Table 7, Fig. 12), evidence for the geochemical affinity of some trace elements and their synchronous involvement in ore emplacement.

The ores are obviously enriched in light REE and depleted in heavy REE with Hf/Sm, Nb/La and Th/La ratios <1 (Table 8). Consequently, the ore-forming fluids belonged to a $NaCl–H_2O$ hydrothermal system enriched in Cl at the expense of F (Oreskes, Einaudi, 1990); this corresponds to our data on FIs in synore quartz (see above). The average Y/Ho ratio of the studied ores is 45.89 (Table 8), typical of

Table 7. Geochemical characteristics of ores of Teploe deposit

Element	Sample numbers and element concentrations, g/t										Avg	EF
	T-2-2	K-19-2	178-2	178-3	Sht. 4	M-3-1	177-1	2925	31205	312		
Au	5.1	3.6	1.6	16	4.3	6.7	5.5	23	13	8.4	8.62	4788.97
Ag	1398	281	71	2894	1281	1169	1161	1839	2344	2421	1485.9	28642.4
Cu	120	96	400	246	110	275	140	273	286	518	246.40	9.85
Mo	<0.018	<0.018	7.1	5.4	<0.018	<0.018	<0.018	24	<0.018	9.1	4.55	3.04
Pb	99	30	229	972	44	24	168	83	127	271	204.76	10.23
Zn	305	352	793	492	125	595	171	1987	625	13489	1893.31	26.66
Cd	1.7	0.49	5.7	2.1	0.45	3.5	0.95	2.40	1.5	152	17.04	173.92
In	0.63	0.36	0.29	0.28	0.35	0.42	0.30	0.29	0.28	0.35	0.35	7.08
Bi	22	2.6	2.0	0.069	2.7	14	8.7	2.3	0.22	4.1	5.86	46.16
As	5.3	10	6.2	0.76	3.0	5.9	2.2	2.3	1.6	2.9	4.06	2.71
Sb	4.2	2.0	2.4	3.2	0.86	2.8	2.4	2.0	8.0	34	6.16	30.79
Sn	2.0	2.2	2.0	1.7	1.5	1.9	1.5	1.3	1.7	3.8	1.95	0.35
W	bdl	bdl	2.0	bdl	bdl	0.13	bdl	5.7	142	52	20.14	10.07
Tl	bdl	0.55	0.015	2.0	bdl	0.009	0.17	bdl	0.16	0.13	0.30	0.4
Te	3.0	1.6	6.0	0.98	1.2	17	0.75	1.2	0.45	1.6	3.33	1.43
Se	0.11	bdl	2.2	1.4	bdl	2.3	0.16	bdl	bdl	bdl	0.61	0.01
Mn	129918	212433	34691	6346	16176	134675	155914	109646	32690	131191	96367.99	160.61
Co	0.25	bdl	bdl	bdl	10	0.087	bdl	1.6	12	5.0	2.94	0.29
Ni	1.1	1.1	2.5	0.44	12	0.60	1.7	4.8	1.9	0.53	2.64	0.13
Li	27	9.0	21	32	41	16	21	82	34	61	34.40	1.72
Rb	<0.027	<0.027	68	<0.027	27	<0.027	<0.027	<0.027	17	125	23.76	0.21
Be	7.6	6.0	7.1	0.86	2.1	6.1	4.2	4.1	2.4	6.5	4.69	1.56
Sc	1.5	2.5	2.6	4.2	13	1.3	0.81	1.8	4.0	0.50	3.20	0.29
Ti	11	5.0	483	115	4962	9.0	30	191	30	27	586.27	0.19
V	12	9.9	30	4.0	92	12	11	61	7.4	28	26.73	0.44
Cr	5.6	10	5.2	11	34	5.4	9.6	293	92	39	50.58	1.44

Table 7. (Contd.)

Element	Sample numbers and element concentrations, g/t										Avg	EF
	T-2-2	K-19-2	178-2	178-3	Sht. 4	M-3-1	177-1	2925	31205	312		
Ga	2.7	0.92	7.1	0.65	11	1.6	1.1	2.5	3.5	16	4.74	0.27
Sr	156	4.8	126	15	501	9.2	7.5	312	132	339	160.19	0.45
Y	12	0.09	21	1.4	14	36	0.04	4.1	0.97	4.7	9.54	0.43
Zr	<0.006	<0.006	22	<0.006	130	<0.006	<0.006	3.6	<0.006	<0.006	15.58	0.08
Nb	<0.003	<0.003	2.1	<0.003	4.2	<0.003	<0.003	<0.003	<0.003	<0.003	0.63	0.02
Ta	<0.001	<0.001	0.28	<0.001	0.16	<0.001	<0.001	<0.001	0.054	<0.001	0.04	0.02
Cs	1.4	0.23	1.8	<0.001	0.92	0.46	0.09	0.02	0.25	12	1.68	0.45
Ba	35	15	311	29	352	63	7.0	17	106	928	186.26	0.33
La	1.7	0.06	11	1.5	16	0.68	bdl	3.9	0.61	3.9	3.95	0.13
Ce	2.6	0.15	24	3.3	36	2.1	0.063	6.9	0.96	2.5	7.81	0.12
Pr	0.73	bdl	3.1	0.53	4.7	0.72	bdl	0.92	0.10	0.33	1.11	0.15
Nd	4.3	0.032	13	2.9	20	5.0	0.004	3.6	0.42	1.3	5.07	0.19
Sm	1.1	0.001	2.7	0.73	3.8	1.7	bdl	0.65	0.068	0.21	1.10	0.24
Eu	0.25	bdl	0.48	0.075	1.2	0.34	bdl	0.16	0.038	0.38	0.29	0.33
Gd	2.0	0.011	3.1	0.71	4.0	2.5	bdl	0.74	0.10	0.30	1.34	0.35
Tb	0.29	<0.0001	0.50	0.055	0.52	0.52	<0.0001	0.082	<0.0001	0.010	0.19	0.30
Dy	2.3	bdl	3.2	0.35	2.9	3.9	bdl	0.60	0.084	0.19	1.34	0.38
Ho	0.49	<0.0002	0.66	0.044	0.52	0.89	<0.0002	0.093	0.009	0.031	0.27	0.34
Er	1.5	<0.0001	2.0	0.15	1.5	2.9	<0.0001	0.30	0.051	0.12	0.84	0.36
Tm	0.19	<0.0001	0.29	0.002	0.19	0.40	<0.0001	0.028	<0.0001	<0.0001	0.11	0.33
Yb	1.3	<0.0001	2.2	0.10	1.3	2.7	<0.0001	0.25	0.050	0.080	0.79	0.35
Lu	0.16	<0.0001	0.30	0.003	0.17	0.38	<0.0001	0.022	<0.0001	<0.0001	0.10	0.32
Hf	<0.003	<0.003	0.72	<0.003	2.8	<0.003	<0.003	<0.003	<0.003	<0.003	0.35	0.06
Th	<0.002	<0.002	4.4	0.01	2.7	<0.002	<0.002	0.13	<0.002	<0.002	0.72	0.06
U	0.026	0.027	1.8	0.15	0.92	0.12	0.002	0.95	0.16	0.50	0.46	0.16

bdl, below detection limit. Trace element concentrations were determined by ICP-MS at IGEM RAS laboratory, analyst Ya.V. Bychkova; Au, by atomic absorption method, analyst V.A. Sychkova; and Ag, by X-ray fluorescence analysis, analyst A.I. Yakushev.

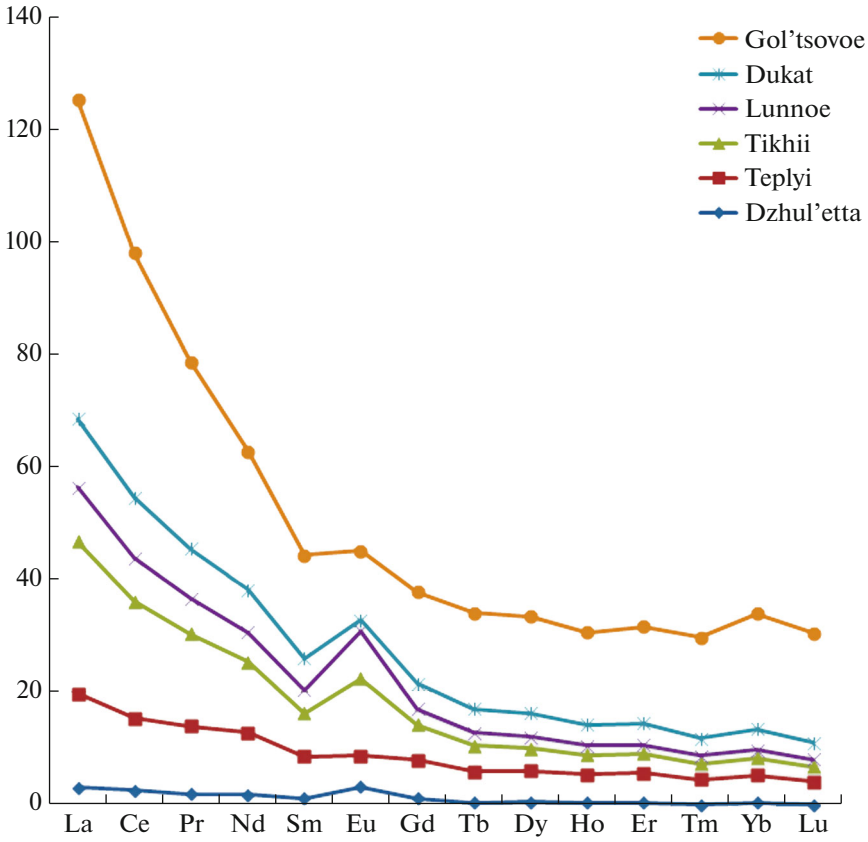

Fig. 13. REE spider plots for ores in epithermal deposits of Omsukchan metallogenic zone.

hydrothermal fluids in back-arc basins (Bau, 1991; Jones, Manning, 1994; Monecke et al., 2002).

The studied ores exhibit fairly low ΣREE values—24.36 on average (Table 8). Equally low sums of REE concentrations are characteristic of epithermal ores of the Omsukchan and other ore regions in the OCVB (Kravtsova, 2010; Volkov et al., 2017) and worldwide (Kurama in Uzbekistan, Banská Štiavnica in Slovakia, and others) (Vinokurov et al., 1999). Note that the sum of the REE concentrations in the studied ores (Table 7) is notably lower than in magmatic and volcanic country rocks in the OCVB (Kravtsova, 2010). The chondrite-normalized average REE values in the ores of the Teplyi area exhibit chondritelike shallow-slope spectra (Fig. 13) largely similar in shape to the REE spectra of country rocks (Kravtsova, 2010).

Eu and Ce anomalies are usually considered markers of the redox potential of the ore emplacement environment (Bortnikov et al., 2007; Goryachev et al., 2008). Samples from ores of the Teploe deposit exhibit negative Eu/Eu* and positive Ce/Ce* values close to 1 except for anomalous sample 312 (Table 8). Such a combination of Eu/Eu* and Ce/Ce* ratios attests to the slightly oxidizing conditions during ore emplacement. Low Eu/Sm ratios (<1) in studied ores (Table 8) suggest that ore formation took place at the upper crustal level (Vinokurov, 1996).

DISCUSSION AND CONCLUSIONS

The distinguishing feature of the deposit is its occurrence at the junction of two crustal blocks, the southern flank of the Omsukchan continental rift and the Okhotsk volcanic zone of the Uda–Murgali volcanic belt. Extending along the strike of these regional structures are two large metallogenic zones—the N–S trending Omsukchan zone characterized by economic Sn, Ag, Pb, and Zn mineralization and the Uda–Murgali zone with Cu and Mo mineralization (Sidorov et al., 2009; Volkov et al., 2014).

Our data on the mineral and chemical composition of the Teplyi area display all signatures of a preporphyry volcanogenic deposit as classified by (Sidorov et al., 2011). Additional Cu supply substantially affected the Ag mineral phases of the late assemblages. Studies of metasomatic ore mineralization made it possible to identify two hypogene mineralization stages—volcanogenic and an overprinted plutonogenic stage.

Early-stage minerals weakly affected by the late heating process are preserved only in surface mining workings on the western flank of the Teplyi area. They

Table 8. Indicators of ores in Teplyi area of Primorskoe deposit

Indicator	Sample number										C
	T-2-2	K-19-2	178-2	178-3	Sht. 4	M-3-1	177-1	2925	31205	312	
ΣREE	18.8	0.2	67.0	10.3	92.5	24.7	0.1	18.2	2.5	9.3	24.36
ΣLREE	10.6	0.2	54.8	8.9	81.4	10.6	0.1	16.1	2.2	8.6	19.35
ΣHREE	8.1	0.0	12.3	1.4	11.1	14.1	0.0	2.1	0.3	0.7	5.01
ΣLREE/ΣHREE	1.31	21.41	4.46	6.35	7.35	0.74	–	7.65	7.46	11.85	6.86
Hf/Sm	–	–	0.26	–	0.72	–	–	–	–	–	0.09
Nb/La	–	–	0.18	–	0.26	–	–	–	–	–	0.04
Th/La	–	–	0.39	0.01	0.16	–	–	0.03	–	–	0.06
Y/Ho	25.30	–	32.54	31.65	27.19	40.89	–	43.91	105.40	152.03	45.89
U/Th	–	–	0.41	10.07	0.34	–	–	7.13	–	–	1.79
Rb/Sr	–	–	0.54	–	0.05	–	–	–	0.12	0.36	0.11
Sr/Ba	4.44	0.32	0.40	0.53	1.42	0.14	1.06	18.42	1.24	0.36	2.83
Zr/Hf	–	–	30.49	–	46.83	–	–	–	–	–	7.73
Nb/Ta	–	–	7.63	–	26.51	–	–	–	–	–	3.41
Co/Ni	0.23	–	–	–	0.86	0.14	–	0.32	6.50	9.60	1.76
Te/Se	27.12	–	2.69	0.72	–	7.21	4.69	–	–	–	4.24
Au/Ag	0.003	0.01	0.02	0.005	0.003	0.005	0.004	0.01	0.005	0.003	0.005
Eu/Eu*	0.71	–	0.63	0.52	1.06	0.60	–	0.87	–	5.06	0.94
Ce/Ce*	0.57	1.51	1.01	0.92	1.10	0.60	–	0.90	0.83	0.34	0.78
La_N/Yb_N	0.91	–	3.55	10.48	8.54	0.16	–	10.61	8.25	33.43	7.59
La_N/Sm_N	1.00	54.51	2.58	1.25	2.58	0.24	–	3.70	5.56	11.86	8.33
Gd_N/Yb_N	1.22	–	1.17	5.99	2.59	0.74	–	2.41	1.63	2.98	1.87
La_N/Lu_N	1.13	–	3.93	51.72	9.65	0.18	–	18.48	–	–	8.51
ΣCe	9.31	0.23	51.56	8.12	76.33	8.52	0.06	15.30	2.09	8.01	17.95
ΣY	6.32	0.01	10.68	1.96	13.04	9.83	0	2.32	0.29	1.11	4.55
ΣSc	2.92	–	4.49	0.24	2.90	5.96	–	0.56	0.10	0.19	1.74
Eu/Sm	0.23	–	0.17	0.10	0.32	0.19	–	0.24	0.55	1.81	0.36
Ce/Yb	1.99	–	10.99	34.29	28.50	0.78	–	27.83	19.17	30.62	15.42
Eu/Ce	0.09	–	0.02	0.02	0.03	0.15	–	0.02	0.03	0.15	0.05

$Eu/Eu^* = Eu_N/(Sm_N*(Tb_N*Eu_N)^{1/2})^{1/2}$); $Ce/Ce^* = Ce_N/((2La_N + Sm_N)/3)$; REE, rare-earth elements; LREE, light REE; HREE, heavy REE; totals for REE groups (Mineev, 1974): cerium, ΣCe; yttrium, ΣY; scandium, ΣSc.

allow the conclusion that the volcanogenic Au–Ag mineralization stage was characterized by the emplacement of ores with Sb mineralization (pyrargyrite and polybasite) and colloform-banded structures, while host rocks were subject to quartz–sericite alteration.

The late stage is characterized by high-temperature metamorphism of the early epithermal veins, sufficient Cu supply, and the presence of Bi-bearing galena and matildite in ores. The homogenization temperatures of fluid inclusions in quartz of this stage widely vary from 120–347°C to 434°C, according to (Struzhkov and Konstantinov, 2005). Signatures of rejuvenation of the ore-forming system have been found. As a result, medium- to high-temperature chlorite–epidote with actinolite facies of contact metasomatites formed simultaneously with garnet–magnetite–rhodonite–epidote mineralization in orebodies, as in the large Dukat Ag–Au deposit (*Serebro* ..., 1989); this was accompanied by removal of Sb and redistribution of Ag, which led to the deposition of a wide variety of Cu and Fe sulfides (Table 2).

As demonstrated earlier (Savva et al., 2016), the composition of volcanic country rock and metallogenic specialization affect the geochemistry and mineral types of deposits. The prevalence of Cu–Ag sulfides, such as jalpaite, stromeyerite, and mckinstryite, as well as Cu-acanthite and Cu-uytenbogaardtite (Table 2), in ores of the Teplyi area reflects the influence of the Uda–Murgali paleoarc, characterized by

Cu–Mo mineralization. Similar interrelations and mineral assemblages were established in other ore deposits in northeastern Russia: the Ol'cha, Nyavlenga, and Dzhul'etta (Savva and Shakhtyrov, 2011; Savva et al., 2007, 2016) and described in detail for the Pallancata deposit in Peru (Jorge et al., 2013). The metallogenic effect of the Omsukchan zone (characterized by Ag–Sn–base metal mineralization) accounts not only for high Ag grades in ores of the Teplyi area (Ag-acanthite mineral type) but also for the wide development of Mn minerals (rhodonite, manganosiderite, and rhodochrosite).

As a result of comparative analysis of geochemical data for ores of the Teplyi area and other Ag–Au deposits of the Omsukchan metallogenic zone (Struzhkov and Konstantinov, 2005), the following common features were established: a wide range of major indicator elements and the presence of Mn among them; elevated W concentrations; high Mn and Ag enrichment factors; high values of Sr/Ba and Y/Ho ratios; a very low Au/Ag ratio; a low ∑REE value; negative Eu and positive Ce anomalies; and similar REE distribution patterns (Fig. 13). The specific geochemical features of ores in the Teplyi area were also established: low S_{total} values, low Pb and Zn and elevated Cu and Bi grades, and high Te/Se ratios— (Table 8).

According to Table 8, light hydrophilic lanthanides of the cerium group prevail in the REE spectra of the studied ores (Zharikov et al., 1999; Mineev, 1974). Host volcanic rocks of the Omsukchan district are characterized by similar REE composition (Kravtsova, 2010). The U/Th and Co/Ni ratios (Table 8) in the studied ores vary widely, suggesting thermal metamorphism of the ores.

New data on fluid inclusions (FIs) in quartz suggest that quartz–rhodonite vein mineralization of the Teploe deposit was formed in several stages at high and medium temperatures (347–120°C) from low-concentration hydrothermal chloride solutions (3.38–0.35 wt % NaCl eq.) saturated with Na and K cations. Note that the physicochemical parameters of ore emplacement in the Teplyi area (Table 5) are unusual as compared with other epithermal deposits of the Omsukchan zone (Struzhkov and Konstantinov, 2005). These include high temperatures and low salt concentrations and fluid densities in fluid inclusions characteristic of "dry vapor", meaning that the ore system was ***overheated*** (the temperature exceeded the critical point of water) at the background of H_2O deficiency. These parameters could also be caused by thermal metamorphism of the ores. The degree of metamorphism in ores is so high that it leads to ore mineral dissolution and redeposition. Ag redistribution leads to the development of more or less ordered exsolution structures in Cu–Ag–S system (Fig. 9c) and Ag–Fe–S lenaite (structural equivalent of chalcopyrite) formation.

Minerals of the Cu–Ag group that are usually rare in occurrence—stromeyerite, jalpaite, and mckinstryite—display a wide range of compositions (Fig. 9c) and a sizable proportion in the studied ores. This is evidence of the spatial and genetic relationship with the porphyry copper mineralization system of the Uda–Murgali metallogenic zone. The obtained data make it possible to classify the Primorskoe as an epithermal intermediate sulfidation deposit (Richards, 2013; Simmons et al., 2005).

The data discussed in this paper are of practical use for regional metallogenic forecasting, exploration, and economic evaluation of epithermal Ag–Au deposits.

FUNDING

This work was supported by the Program of Presidium of Russian Academy of Sciences (no. 48 "Deposits of Strategic and High-Tech Metals in the Russian Federation: Spatial Distribution, Formation Conditions, and Innovative Forecast, Exploration, and Mining Technologies"), the State Assignment project for Institute of Geology of Ore Deposits, Petrography, Mineralogy, and Geochemistry, Russian Academy of Sciences (no. 0136-2018-0022 "Metallogeny of Ore Districts in Volcanogenic, Plutonogenic, and Folded Orogenic Belts of Northeastern Russia"), and the Russian Science Foundation (project no. 14–17–00170).

CONFLICT OF INTEREST

The authors declare that they have no conflict of interest.

REFERENCES

Bau, M., Rare-earth element mobility during hydrothermal and metamorphic fluid-rock interaction and the significance of the oxidation state of europium, *Chem. Geol.,* 1991, vol. 93, pp. 219–230.

Bodnar, R.J. and Vityk, M.O., Interpretation of microterhrmometric data for H_2O–NaCl fluid inclusions, *Fluid Inclusions in Mminerals: Methods and Applications,* Siena: Pontignano, 994, pp. 117–130.

Borisenko, A.S., Cryometric study of salt composition of gas–liquid inclusions in minerals, *Geol. Geofiz.,* 1977, no. 8, pp. 16–27.

Bortnikov, N.S., Gamyanin, G.N., Vikent'eva, O.V., et al., Fluid composition and origin in the hydrothermal system of the Nezhdaninsky gold deposit, Sakha (Yakutia), Russia, *Geol. Ore Deposits,* 2007, vol. 49, no. 2, pp. 87–128.

Brown, P., Flincor: a computer program for the reduction and investigation of fluid inclusion data, *Am. Mineral.,* 1989, vol. 74, pp. 1390–1393.

Goryachev, N.A., Vikent'eva, O.V., Bortnikov, N.S., et al., The world-class Natalka gold deposit, Northeast Russia: REE patterns, fluid inclusions, stable oxygen isotopes, and formation conditions of ore, *Geol. Ore Deposits,* 2008, vol. 50, no. 5, pp. 362–390.

Jorge, E., Ricardo, C., Heinz-Jürgen, B., Preliminary mineralogy and ore petrology of the intermediate–sulfidiation Pallancata deposit, Ayacucho, Peru, *Can. Mineral.,* 2013, vol. 51, pp. 67–91.

Kravtsova, R.G., *Geokhimiya i usloviya formirovaniya zolotoserebryanykh rudoobrazuyushchikh sistem Severnogo Priokhot'ya* (Geochemistry and Conditions of Formation of Gold–Silver Ore-Forming Systems of the Northern Okhotsk Region), Novosibirsk: "Geo", 2010.

Kryazhev, S.G., Prokof'ev, V.Yu., and Vasyuta, Yu.V., Application of ICP-MS for analysis of composition of ore-forming fluids, *Vestn. Mosk. Univ., Ser. 4. Geol.,* 2006, no. 4, pp. 30–36.

Manning, D.A.C., Comparison of geochemical indices used for the interpretation of palaeoredox conditions in ancient mudstones, *Chem. Geol.,* 1994, vol. 111, pp. 111–129.

Mineev, D.A., *Lantanoidy v rudakh redkozemel'nykh i kompleksnykh mestorozhdenii* (Lanthanides in Ores of the Rare-Earth Element and Complex Deposits), Moscow: Nauka, 1974.

Monecke, T., Kempe, U., and Gotze, J., Genetic significance of the trace element content in metamorphic and hydrothermal quartz: a reconnaissance study, *Earth. Planet. Sci. Lett.*, 2002, vol. 202, pp. 709–724.

Oreskes, N. and Einaudi, M.T., Origin of rare-earth element enriched hematite breccias at the Olympic Dam Cu–U–Au–Ag deposit, Roxby Downs, South Australia, *Econ. Geol.,* 1990, vol. 85, no. 1, pp. 1–28.

Panet, I., et al., Mapping the mass distribution of earth's mantle using satellite-derived gravity gradients, *Nature Geosci.,* 2014, vol. 7, no. 2, p. 131.

Prokof'ev, V.Yu., *Geokhimicheskie osobennosti rudoobrazuyushchikh flyuidov gidrotermal'nykh mestorozhdenii zolota razlichnykh geneticheskikh tipov* (Geochemical Features of Ore-Forming Fluids of Hydrothermal Gold Deposits of Different Genetic Types), Novosibirsk: Nauka, Sibirskaya izdatel'skaya firma RAN, 2000.

Prokof'ev, V.Yu. and Pek, A.A., Problems in estimation of the formation depth of hydrothermal deposits by data on pressure of mineralizing fluids, *Geol. Ore Deposits,* 2015, vol. 57, no. 1, pp. 1–20.

Richards, J.P., Giant ore deposits formed by optimal alignments and combinations of geological processes, *Nature Geosci.,* 2013, vol. 6.

Savva, N.E., and Shakhtyrov, V.G., The Ol'cha gold–silver deposit: tectonic setting, structure, and mineralogy, *Geol. Ore Deposits,* 2011, vol. 53, no. 5, pp. 412–433.

Savva, N.E., Sidorov, A.A., and Volkov, A.V., Cu–Ag sulfides as indicators of pre-porphyritic epithermal Au–Ag deposits in Northeastern Russia, *Dokl. Earth Sci.,* 2016, vol. 469, pp. 782–786.

Savva, N.E., Volkov, A.V., and Sidorov, A.A., Thermal metamorphism of Au–Ag ores of the Nyavlenga Deposit (Northeast Russia), *Dokl. Earth Sci.,* 2007, vol. 413, pp. 370–375.

Serebro. Geologiya, mineralogiya, genezis, zakonomernosti razmeshcheniya mestorozhdenii (Silver. Geology, Mineralogy, Genesis, and Distribution of Deposits), Moscow: Nauka, 1989.

Sidorov A.A., Belyi V.F., Volkov A.V., et al., The gold–silver Okhotsk–Chukotka volcanic belt, *Geol. Ore Deposits,* 2009, vol. 51, no. 6, pp. 441–455.

Sidorov, A.A., Starostin, V.I., and Volkov, A.V., *Rudnoformatsionnyi analiz* (Ore Formation Analysis), Moscow: MAKS Press, 2011.

Simmons, S.F., White, N.C., and John, D.A., Geological characteristics of epithermal precious metal and base metal deposits, *Econ. Geol.,* 2005, vol. 100, pp. 485–522.

Struzhkov, S.F. and Konstantinov, M.M., *Metallogeniya zolota i serebra Okhotsko-Chukotskogo vulkanogennogo poyasa* (Gold and Silver Metallogeny of the Okhotsk–Chukotka), Moscow: Nauch. mir, 2005.

Taylor, S.R. and McLennan, S.M., *The Continental Crust: its Composition and Evolution,* Oxford: Blackwell, 1985.

Vinokurov S.F. Europium Anomalies in Ore Deposits and Their Geochemical Significance, *Dokl. Earth Sci.,* 1996, vol. 347, pp. 281–283.

Vinokurov, S.F., Kovalenker, V.A., Safonov, Yu.G., et al., REE in quartz from epithermal gold deposits: distribution and genetic implications, *Geochem. Int.,* 1999, vol. 37, no. 2, pp. 145–152.

Volkov A.V., Murashov K.Yu., and Sidorov A.A. Geochemical Patterns of Epithermal Ore Formation in the Okhotsk–Chukotka Volcanoplutonic Belt (Northeast Russia), *Dokl. Earth Sci.,* 2017, vol. 474, pp. 595–598.

Volkov, A.V., Sidorov, A.A., and Starostin, V.I., *Metallogeniya vulkanogennykh poyasov i zon aktivizatsii* (Metallogeny of Volcanogenic Belts and Activation Zones), Moscow: OOO "MAKS Pres", 2014.

Zharikov V.A., Gorbachev N.S., Lightfoot, P., et al., Rare earth element and yttrium distribution between fluid and basaltic melt at pressures of 1–12 kbar: evidence from experimental data, *Dokl. Earth Sci.,* 1999, vol. 366, pp. 543–545.

Translated by E. Murashova